Computational Methods in the age of Materials Informatics: Discovery and Design of Novel 2D Compounds for Spintronic Applications

Gabriel de Miranda Nascimento* and Gustavo Martini Dalpian†
Center for Natural and Human Sciences
Federal University of ABC
(Dated: July 21, 2022)

In the past decades, the development of electronic structure methods, mainly within the formalism of Density Functional Theory (DFT), has evolved in terms of predictive power and efficiency, being highly spread over the entire field of materials modeling and condensed matter physics and providing large support for understanding and complementing experimental efforts in this area. When coupled with the increasing supercomputing power and resources available in recent years, these computational methods are reaching an inflection point that enables them to explore large portions of the materials landscape that were even unknown to humankind, fostering and accelerating materials design and discovery for the next generation technological applications. In this work, we implement these methods to the identification and study of novel 2D materials specifically targeted for applications in spintronic devices. By exploring the so-called spin-splitting (SS) effects that emerge in these special classes of materials, the spin polarization degrees of freedom of these system's electronic states can then be controlled, providing additional ways for the manipulation and read-out of digital information, in a novel type of (spin) electronic devices. More specifically, we have developed a fully automatic computational workflow for the inverse design of materials with the target functionalities, performing DFT calculations for hundreds of compounds and identifying 358 materials displaying promising SS effects in their valence and conduction bands. Moreover, we fully characterize the 1267 different SS effects found in these materials both in terms of the effective models that describe them and the metrics that provide their feasibility for real applications. An extensive computational database of SS in 2D materials is then constructed and made openly available, and is aimed at supporting new research efforts on the design and development of new devices. The information here available, encapsulating a wide range of the materials landscape, can shine light on important trends and correlations that guide the mechanisms behind the emergence of SS effects and its possible control, supporting new theoretical studies on the interplay of these effects with the other materials properties, in addition to being able to serve as an initial guide for the rational choice of compounds to experimental verifications and implementation in new devices.

I. INTRODUCTION

The development made in the fields of solid state/condensed matter physics over history, with its fundamental theoretical methodologies for understanding and quantifying quantum systems, has only in the past few decades met the increasing power of high-performance computing (HPC) and more recently big data and artificial intelligence (AI) aided methodologies [1]. The result of this combination may lead to a shift in perspective about how novel materials for specific applications are designed, overcoming the traditional discovery approach, generally based on trial and error, and paving the way for a more systematic and predictive strategy, which is responsible for radically accelerating the rate of technological developments and innovation.

Such a shift in perspective is primarily possible due to the development of electronic structure methods with increasingly accuracy [2, 3], mainly within the framework of DFT (see Appendix A for an introduction on the theory supporting these methods), that are helping to bridge the gap between experiments and the theoretical understanding [4]. The predictive power provided by these developments grounds the basis for the computational design and discovery of materials, and the application of these methods in a systematic, large scale and HPC environment is at the core of the rapid-growing field of Materials Informatics [5, 6].

An expressive result of such research efforts is the emergence of multiple computational materials databases [7–11], that already encompass, curate, and make available information about an increasingly large portion of all crystalline materials known by mankind, structuring resources and fostering large-scale studies to identify and inverse-design materials targeted for various applications [12].

In this context, the class of two-dimensional materials has been gaining increasing attention as a fast-growing area of application of such computational efforts in materials design. Due to its relatively recent discovery, with the first isolation of graphene by mechanical exfoliation in 2004 [13] leading up to the Nobel Prize in Physics six years later, the number of known and already synthesized 2D compounds is still infinitesimally small when

* nascimento.gabriel@aluno.ufabc.edu.br
† gustavo.dalpian@ufabc.edu.br

compared to its known 3D-bulk counterparts, which have been systematically studied and employed in all areas of technological applications throughout human history. In this sense, the traditional extensive trial and error approach, based on experimental synthesis and study of many possible new compounds until the discovery of promising ones for specific applications, can be readily accelerated by computational methods of materials simulations. These approaches have increasing capabilities of exploring large portions of the materials landscape, previously unknown by mankind, in an exponentially faster way when compared to the traditional approach. In this manner, with the data generated by those efforts, only the most promising material candidates can undergo experimental scrutiny, being then physically realized and employed in real applications and devices.

In this perspective, since the nascence of the field of 2D materials, computational methods have been extensively developed to identify other possible layered compounds that could be exfoliated by similar means to graphene [14–18]. These algorithms, designed to scan computational crystal databases and identify graphite-like layered materials for mechanical exfoliation, could soon outreach, in orders of magnitude, the sheer amount of layered materials candidates verified solely with experimental trial and error efforts.

With this large number of possible new 2D structures, robust computational frameworks [19, 20], based on DFT simulations, have successfully been applied to predict, from first principles, a wide range of properties for these compounds [21]. Initially, they can in this way have a measure of its stability addressed in different ways [22], in order to have a safe estimation of its feasibility of experimental realization. Moreover, these approaches are known to generate new compounds distributed across a wide range of electronic and magnetic properties, which can be exploited in different technological applications in devices.

Other methods for materials generation, such as prototyping, i.e chemical substitution, have also collaborated to the exponential growth of the number of theoretical proposed 2D materials, leading to the creation of specialized databases for two-dimensional structures [23–25]. These databases, which now share tens of thousands of possibly novel materials, start to present themselves as central supporting resources for a wide variety of computational efforts, from large-scale studies of different properties and functionalities suited for various applications [26], to implementation in AI and machine learning models [27, 28].

With this perspective, the different classes of 2D materials have soon extended the path for novel applications in various fields, such as electronics and optoelectronics [29]. Due to the endless possibilities of arranging these compounds into van der Waals (vdW) heterostructures [30] in a controlled and thoughtful manner, these types of assemblies represent a rich platform for the development of devices that have their properties carefully modulated for specific applications of interest.

In this context, a potential area of application of such devices is within the fast-growing field of spintronics, which aims at the construction of a novel electronics technology based on the spin degrees of freedom of electrons. In analogy to electronic transistors, these spintronic devices aim at controlling the spin polarization of the system's electronic states in order to store and manipulate digital information [31, 32]. This, in principle, could be made by employing materials that display broken spin degeneracies at specific electronic states, having non-zero expected values for the spin polarization that could potentially be explored in such devices for the control and read-out of logical signals [33].

Indeed, Gmitra and Fabian have proposed a vdW-heterostructure based on a bi-layer graphene (BLG) stacked on top of a WSe_2 monolayer which could be effectively employed as a spin transistor in that manner [34]. In their work, they have shown how proximity fields, induced by spin-orbit coupling effects from WSe_2, are able to generate a splitting on the valence bands of the BLG system, in such a way that they are no longer spin degenerate. These states now have specific spin polarization patterns, which can then be controlled by an applied perpendicular electric field, as the publication shows.

With this perspective, one of the main questions the present work addresses is how computational workflows of materials simulations can be applied to identify the largest possible number of 2D materials that can potentially be employed in new devices for spintronic technology. This large-scale materials identification effort is initially translated into the high-throughput study of spin-splitting effects that can emerge in these systems, as they could be the mechanisms used for the discrimination of the different spin-polarized states in these devices.

This paper is therefore structured as follows. We first start by elucidating the physical description of the spin-splitting effects, in Sec. II, that represent the main properties of study in this work to guide the identification of materials for spintronic devices. In short, the establishment of the different effective models for spin-splittings in crystalline systems is the foundation of the posterior materials analysis made here. In Sec. III, the different methods, computational tools, and developed algorithms are described in detail, providing a complete framework for the high-throughput computational search of 2D materials for these applications and study of its spin-splitting properties. Sec. IV then provides an overview of the extensive results from this computational approach, identifying hundreds of novel 2D materials which have their spin-splitting systematically characterized. This section is followed by a discussion of one of the possible mechanisms behind systems with large spin-splitting effects, which are of special interest for applications. A computational database has been constructed to curate this emerging new catalog of spin-splitting effects in 2D materials and a complete guide on accessing these data is then available in Sec. V. Finally, Sec. VI provides an

overview of the role these computational methods play in accelerating materials design for these technological applications of interest and how the results from this work can be used to support both further theoretical investigations and serve as a guide for experimental verifications and new efforts for implementations in devices.

II. PHYSICAL DESCRIPTION OF SPIN-SPLITTING EFFECTS

The understanding of how particular symmetries are broken in quantum systems and how it, in turn, may influence the spin degeneracy in particular energy bands represent some of the foundations of the understanding of spin-splitting (SS) effects, which can play a major role in the operation of spintronic devices [35]. In this context, the interplay of two major discrete symmetries, the spacial inversion and time reversal symmetries, contribute to the description of the degeneracy of the spin states.

On one hand, the presence of spatial inversion symmetry, e.g. due to a scalar potential that satisfies $V(\vec{r}) = V(-\vec{r})$, shows the invariance of the system's properties (i.e. its Hamiltonian) with respect to the change $r \to -r$. It, therefore, implies that its eigenstates (denoted by ε) correspondent to a wavevector $\vec{k}$ and a specific spin (e.g. $\uparrow$) should be energy degenerated with respect to the eigenstate with opposite wavevector and same spin state ($-\vec{k}\uparrow$), yielding:

$$\varepsilon_{\vec{k}\uparrow} = \varepsilon_{-\vec{k}\uparrow}. \tag{1}$$

Similarly, time reversal symmetry expresses the system's invariance with respect to the transformation $t \to -t$. By considering that spin transforms as angular momentum, it is reversed in direction with the reversal in time. In this manner, this symmetry invariance implies the system eigenstates $\varepsilon_{\vec{k}\uparrow}$ and $\varepsilon_{-\vec{k}\downarrow}$ to be energy degenerated, in the form:

$$\varepsilon_{\vec{k}\uparrow} = \varepsilon_{-\vec{k}\downarrow}. \tag{2}$$

The breaking of the spin degeneracy, in this perspective, can then be understood as an interplay of the breaking of its associated symmetries. Figure 1 illustrates this relation for a free-electron model with parabolic bands. As it can be seen, the breaking of time-reversal symmetry, e.g. with the introduction of an external magnetic field, results in the breaking of the degeneracy with a shift in energy from bands with opposite spin polarization. The braking of the inversion symmetry, e.g. with the introduction of an external electrical field, on the other hand, can be associated with a shift-in-k dispersion among bands, with resulting spin polarization textures in such a way that the remaining symmetries are preserved (Fig. 1).

While these breakings of spin degeneracy, i.e. spin-splitting effects, have been initially proposed in atomic systems in the presence of applied external fields, and successfully described under the quantum mechanical formalism of perturbation theory [36], it has been also shown that local electric dipoles and the breaking of particular crystal symmetries could intrinsically induce SS effects [37].

In such context, the spin-orbit coupling (SOC) terms, which are usually the leading terms in relativistic corrections, coupled with a periodic system structure that lacks inversion symmetry, play the major role that leads to the breaking of symmetries that induce SS effects. The historical understanding of these phenomena, together with the different underlying mechanisms at play and proposed effective hamiltonians, leads to the classification of different SS effects, which we here refer to as *SS prototypes*, namely:

1. *Zeeman*: SS induced at k-points without time-reversal point-group symmetry [38, 39].
2. *Rashba*: breaking of the inversion symmetry by the presence of an electric dipole [40–42].
3. *Dresselhaus*: the non-electric breaking of inversion symmetry [43].

These theoretical models also show symmetry constraints of the allowed regions where SS effects happen in reciprocal space, and predict differences in the spin texture in the proximity of those k-points, that is, patterns for the expected values of the spin-polarization projections across the band structure. For instance, both Rashba and Dresselhaus effects are characterized by degenerated states at time-reversal invariant momentum (TRIM) k-points, where bands with opposite spin polarization are dispersed in opposite directions in neighboring k-points, while Zeeman-type spin splitting is known to display non-degenerate bands at non-TRIM k-points [35]. As it is going to be further discussed, these band displacements represent a direct and useful way of computationally classifying the different types of spin splittings in real materials.

Regarding spin texture, Rashba SS displays a helical orientation of spins while Dresselhaus spin polarization is such that it is parallel to its wavevectors when $k_x, k_y = 0$. Zeeman-type SS displays spin polarization projected perpendicular to both k_x, k_y wavevectors (Fig. 2).

These physical phenomena provide emerging functionalities that can be explored in spintronic devices, on traditional source/switch/detector assemblies, as also mentioned in the previous section. However, unlike with bulk 3D crystalline compounds, the current lack of curated data and dedicated databases for 2D materials with specific SS properties may be a factor that hinders the possibilities for developments in such devices.

Therefore, the next sections are dedicated to the methods for high-throughput identification of 2D compounds that possess intrinsic SS effects, culminating in the construction of a novel database of SS in 2D materials. Here, computational algorithms are developed to classify the

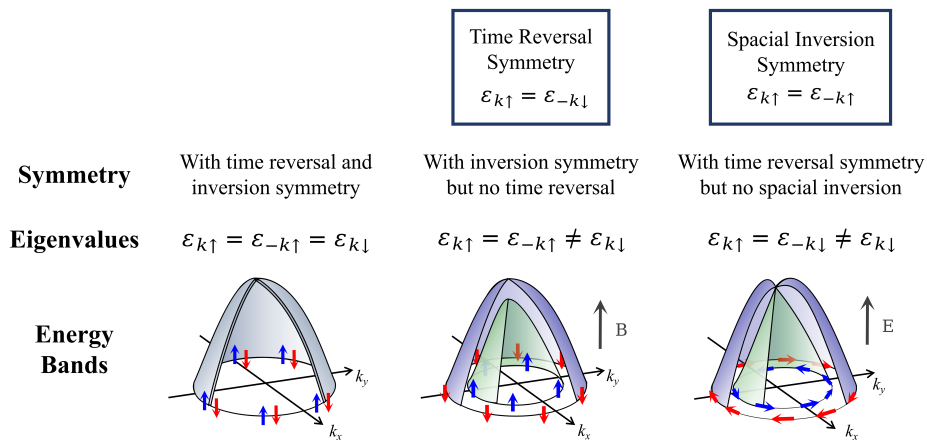

FIG. 1. Interplay of the breaking of time reversal and spatial inversion symmetries with the spin degeneracy and polarization texture in a free-electron band model.

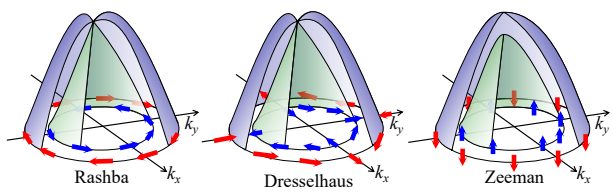

FIG. 2. **Spin splitting prototypes.** Representation of SS prototypes and its characteristic spin polarization and band displacement of a parabolic band representation in a two-dimensional Brillouin zone. The reciprocal lattice vectors are referred to as k_x and k_y and the arrows represent the expected value and direction of spin polarization in the main (purple) and neighboring (green) bands. The negative sign for the effective mass in this band representation suggests the behavior of a valence band maximum in a traditional semiconductor, but an analogous representation of the CBM can be made. Figure extracted from ref [35], with the authors' permission.

selected compounds according to the aforementioned SS prototypes and measure SS quantities and coefficients that address their expected performance and feasibility. An extensive analysis of orbital contributions and anti-crossing effects are also made to verify their influence on the SS properties of the compounds.

III. THE DEVELOPED HIGH-THROUGHPUT COMPUTATIONAL WORKFLOW

This section is dedicated to the methods and computational frameworks developed for the study and identification of SS effects in 2D materials at a large scale. It starts by describing the starting data of two-dimensional structures analyzed and the screening process used to filter the material candidates that possibly display the SS properties of interest in this work. We then describe the workflow of DFT calculations constructed to compute the required data for SS identification in these compounds, consisting of their band structures with spin texture resolution. Finally, we show the design principles that have been employed in the construction of a novel computational code for automatic identification and classification of SS effects in materials band structures, employed for the high-throughput characterization of SS properties in hundreds of 2D compounds, which are originally proposed in this work to possible spintronic applications.

A. Computational data source and screening process

The data source for two-dimensional structures employed in the high-throughput workflow was the Computational 2D Materials Database (2020 version) [44], containing a total of 3814 unique entries generated by elemental substitution based on known 2D structure prototypes. With these starting data, all the entries were scanned with a modified rank determination algorithm, proposed by ref. [45] and implemented in the `analysis.dimensionality` python module from by Pymatgen [46], in order to certify that all compounds in the workflow were composed of cohesive 2D structures.

At this point, 3708 materials classified as 2D by the algorithm proceed in the workflow. According to the fundamental constraints for the SS properties of interest, as well as additional criteria for feasible applications in devices, we construct a set of *Enabling Design Principles*, that represent the necessary conditions that are fundamental to the SS effects and for the context in which these materials are intended to be employed. This set of criteria is applied as filters to the raw data to select material candidates that can possibly display SS effects,

then entering into the next steps of the computational workflow. They are represented below:

1. **Non-zero electronic band gap:** Materials suited for applications in semiconductor devices (1020 entries)

2. **Non-centrosymmetric structure:** Select only structures that lack inversion-symmetry, as a necessary condition for intrinsic SOC-inducing SS effects (501 entries)

3. **Non-magnetic materials:** Non-trivial magnetic ordering is not encompassed by the SS models defined in this analysis. Only non-magnetic compounds are kept in the workflow. (437 entries)

The remaining 437 entries from the screening process proceed in the workflow to the computation of SS properties.

B. *Ab-initio* electronic structure calculations

The intrinsic SS properties of materials can be verified with the computation of its band structure with spin texture resolution. Therefore, we have employed a framework of ab-initio calculations based on Density Functional Theory (DFT), with relativistic corrections for accounting for SOC effects, being essential to the observation of emergent SS phenomena as described above. The workflow is constructed with the Vienna Ab-initio Simulation Package (VASP) for the DFT computations, with the frozen-core all-electron projector-augmented wave (PAW) method [47–49]. The exchange-correlation functional employed in all calculations is the GGA-PBE [50], and the pseudopotentials applied for each element are chosen according to Materials Project [51] standard workflow recommendation. The automation and management of the computational workflow are performed with the ASE Python package [52], which includes plug-ins for interfacing with VASP. Parsing results and post-analysis are done with various tools available in Pymatgen package [46].

The calculations in the workflow are then designed in subsequent steps to provide the final band structure result for each material. These steps are divided into three DFT calculations, namely:

(i) **scf_std**: self-consistent calculation for generating the initial charge density.

(ii) **scf_ncl**: self-consistent calculation for optimizing the initial charge density accounting for SOC.

(iii) **bands_ncl**: non-self-consistent, non-collinear calculation for computing the Kohn-Sham eigenvalues along specific paths in the Brillouin zone, generating band structures with spin resolution.

Throughout all calculations, an energy cutoff of 520 eV was used for the plane-wave expansion of the Kohn-Sham wavefunctions, while electronic convergence has been achieved within 10^{-6} eV. In the self consistent calculations (namely, the `scf_std` and `scf_ncl` ones) k-point sampling has been dealt in a Γ centered grid Monkhorst-Pack grid [53, 54] of 11x11x1 k-points. It is noted that the only difference among these first two calculations is the non-collinear scheme for the latter case. For the non-self-consistent calculation (i.e. the iii one) the method provided by `ASE` [52] for the sampling of Brillouin Zone according to the high-symmetry k-paths was employed, with a density parameter of 80 k-points per Å^{-1}, set for all compounds.

No relaxation procedure was made necessary, once the available structures in the database already correspond to an energy minimum, according to the same xc-functional employed throughout the calculations both in the database and in this work, as it has been verified for a sample of entries in the start of the workflow.

Throughout the DFT calculations workflow, the compound with the chemical formula Au_2Te_2 (band gap of 0.04 eV according to the C2DB database) was perceived as metallic according to the GGA-PBE calculations implemented in this work, so it did not proceed to the SS identification analysis. As it will be further discussed, the band structures with spin resolution obtained in the calculations for all the resulting 436 materials in this work are available in an online repository from the Materials Cloud infrastructure [7, 55]

C. SS identification algorithm

With all the data that was generated throughout the workflow, a computational algorithm have been developed to automatically i) scan all materials band structures ii) identify the SSs that happen in each material valence and conduction bands, and iii) classify each SS according to the spin splitting prototype aforementioned (see Fig. 2). Additionally, a large number of materials have been identified as displaying SS effects whose bands dispersion, in principle, could not be fitted by one of the linear-in-k effective models previously presented. To still keep such materials in the analysis, a fourth category of SS prototype was created, being the *High-Order* SS prototype, to encompass the observed SS effects that can not be directly modeled by the effective Hamiltonian of the other SS prototypes, i.e. which would need higher orders of k (e.g. k^2, k^3...) to be correctly fitted.

The classification of the SS in the materials band structure then follows simple heuristics in order to fit the identified SS into the models that represent the Rashba, Dresselhaus, Zeeman, and High-order prototypes. It is based on specific criteria, referred to in this work as *unique design principles*, that consider i) the structure symmetry, indicating the presence of possible non-vanishing electric dipoles in the material's structure, ii) the symmetry of

the k-point where the SS occurs, identifying if it represents a time-reversal invariant momentum (TRIM) or non-TRIM wavevector, and iii) the band dispersion in the neighboring region of the k-point where the SS occurs, analyzing if it would fit a linear-in-k Rashba/Dresselhaus Hamiltonian or a higher-order Hamiltonian. A schematic diagram of the logical process implemented in the algorithm is presented in Fig. 3.

The developed algorithm, implemented in Python, is openly available in a GitHub repository of this work (github.com/simcomat/SS_2D_Materials). It enables not only the full reproducibility of the findings further highlighted, but also it has the potential of being applied to other classes of materials, supporting the identification and study of SS effects in other compounds and the resulting enlargement of materials with the potential to be employed in new spintronic devices.

IV. RESULTS AND DISCUSSION

The automatic scanning of the algorithm on all the remaining materials in the workflow yields a total number of 1267 different SS identified in the valence and conduction bands of 358 different compounds, which are distributed in the SS prototypes according to Table I. For each identified SS, the SS magnitude ΔE_{SS}, i.e. the energy difference between non-degenerate polarized states, and the energy difference between the SS and the VBM/CBM ($\Delta E_{VBM/CBM}$) are measured. These parameters are of large importance for estimating the performance of the material in a spintronic device, as the former has a direct indication of the possible discrimination of the different spin states under the device operation, and the latter is a parameter to estimate the likelihood of the SS be experimentally verified. For the cases where a Rashba/Dresselhaus SS is identified, its associated coefficient ($\alpha_{R,D}$) is also computed, according to equation 3:

$$\alpha_{R,D} = 2\frac{\Delta E_{SS}}{\Delta \vec{k}}, \tag{3}$$

which is the ratio between the SS magnitude (ΔE_{SS}) and the wavevector displacement over the reciprocal space ($\Delta \vec{k}$) of the SS, and represents an important parameter for accessing the overall intensity of the SS effect in those cases.

SS prototype	# SS
Rashba	205
Dresselhaus	62
Zeeman	488
High-Order	519

TABLE I. Distribution of the identified SS according to the proposed prototypes.

The SS analysis, therefore, presents a handful number of promising candidates for spin-related applications, proposing compounds previously unknown to display such effects and also identifying already reported 2D materials, such as MoS_2 and WSe_2, that are known for the Zeeman effect [56, 57]. Figure 4 provides examples of band structures of real compounds identified by the algorithm as possessing SS effects classified across the different SS prototypes established in this work. Additionally, Section V provide extensive information about the generated data and the different ways it can be acessed.

A. Effect of anti-crossing bands

The systematic and extensive identification of spin-splitting effects in 2D materials provides a rich source of data that may not only support the exploration of possible trends in the materials landscape but also help to guide insights into the physical mechanisms at play in the observed effects. Moreover, regarding the initial evaluation of the different SS targeted to specific applications, one should often consider different metrics that characterize the SS both in its potential for experimental verification and also implementation in a physical device. The understanding of the mechanisms that influence these properties is therefore important, as well as how these different metrics can be related to each other.

Concerning materials that possess Rashba and Dresselhaus-type SS, large $\alpha_{R,D}$ coefficients are of special interest, that is, having large energy dispersion and SS magnitude over a short momentum displacement in the reciprocal space. With this perspective, Acosta *et al.* [58] have demonstrated that the presence of anti-crossing (AC) bands have a causal effect on the magnitude of the Rashba coefficient. These are characterized by the exchange of orbital character in a given pair of energy bands, separated by a forbidden region represented by an energy gap, as illustrated in Figure 5.

In order to verify this important design principle and to understand the physical mechanisms behind materials with robust SS effects, we develop a computational algorithm to scan neighboring spin splittings in the valence and conduction bands, analyze their orbital contributions and determine whether anti-crossing effects are present among the interactions between these bands. Figure 6 illustrates the dispersion of materials according to the SS parameter $\alpha_{R,D}$ and its band gap, according to the presence of anti-crossing effects in the spin split bands.

These results indicate that the presence of AC bands may indicate a sufficient condition for large Rashba coefficient compounds, as all SS possessing AC effects have large values for $\alpha_{R,D}$, but it is not a necessary one, as other materials with large coefficients but the absence of AC effects are also observed.

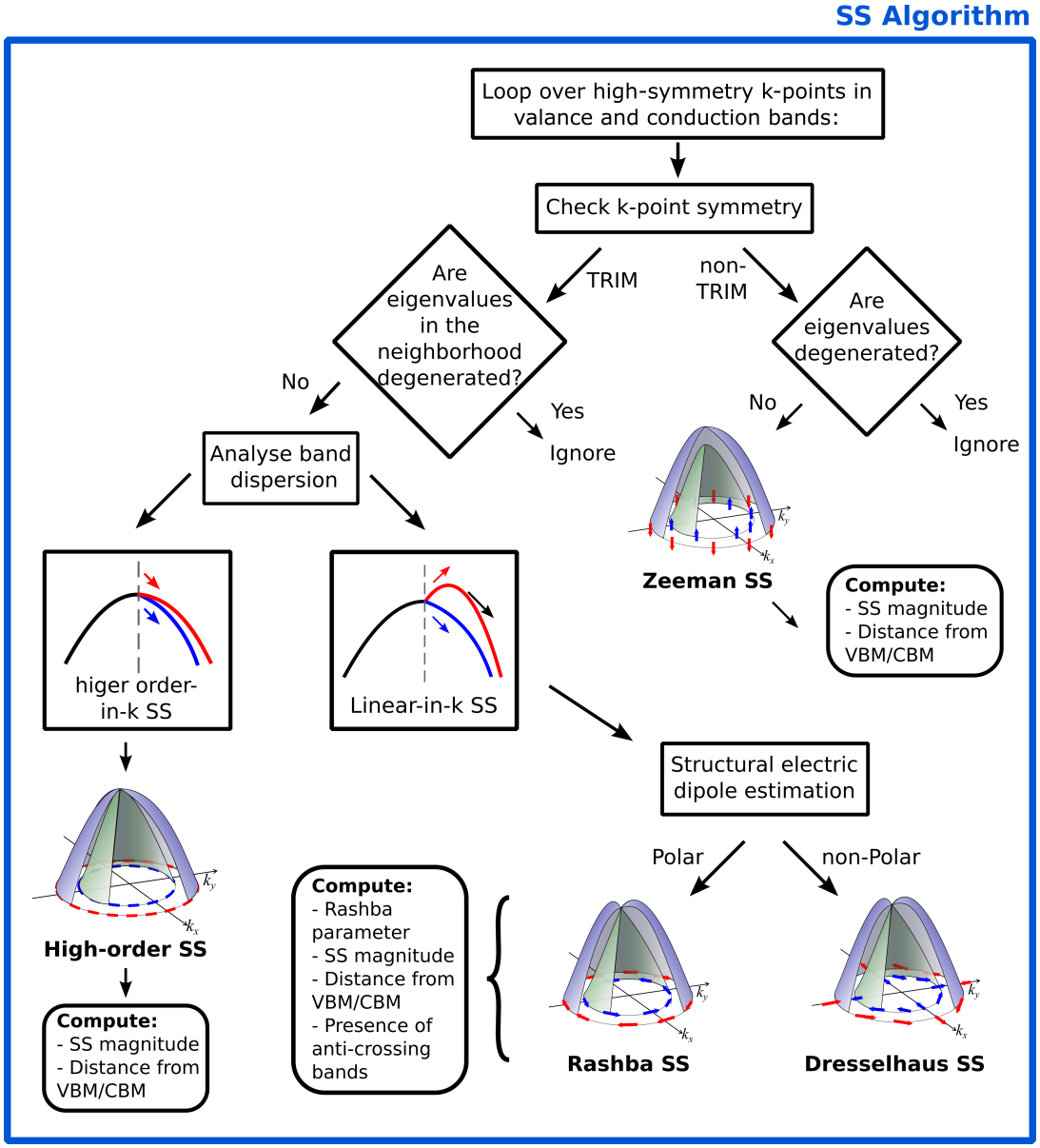

FIG. 3. Diagram representing the logical workflow implemented in the algorithm for SS identification and classification according to the SS prototypes.

V. DATA AVAILABILITY

All the data generated in this high-throughput approach makes it possible for the construction of a novel computational database exclusive to the characterization of spin-splitting effects in 2D materials, reporting hundreds of SS effects in hundreds of different compounds that could be explored in new research efforts of spintronic devices design. Moreover, this enormous amount of information imposes a challenge to make all the data available in a structured way, such as to support its accessibility and usability in those efforts. For this reason, a range of different formats and data structures have been employed in this work to make all the data readily available for different purposes and use cases.

Firstly, an overview of this work's main findings can be found in the Appendix B section at the end of this thesis. They are presented in the form of tables which gather the full list of the identified SS effects for all materials in this work, divided according to SS prototype, including its important metrics that were measured by the algorithm (i.e. ΔE_{SS}, $\Delta E_{VBM/CBM}$, $\alpha_{R,D}$ ...). They also provide general information regarding the different materials that host these SS effects, e.g. the compound's ID in the original database, and some of its relevant properties, e.g. the electronic band gap, structure's symmetry (space group index), and energy above convex hull.

Further than that, an entire online repository has been

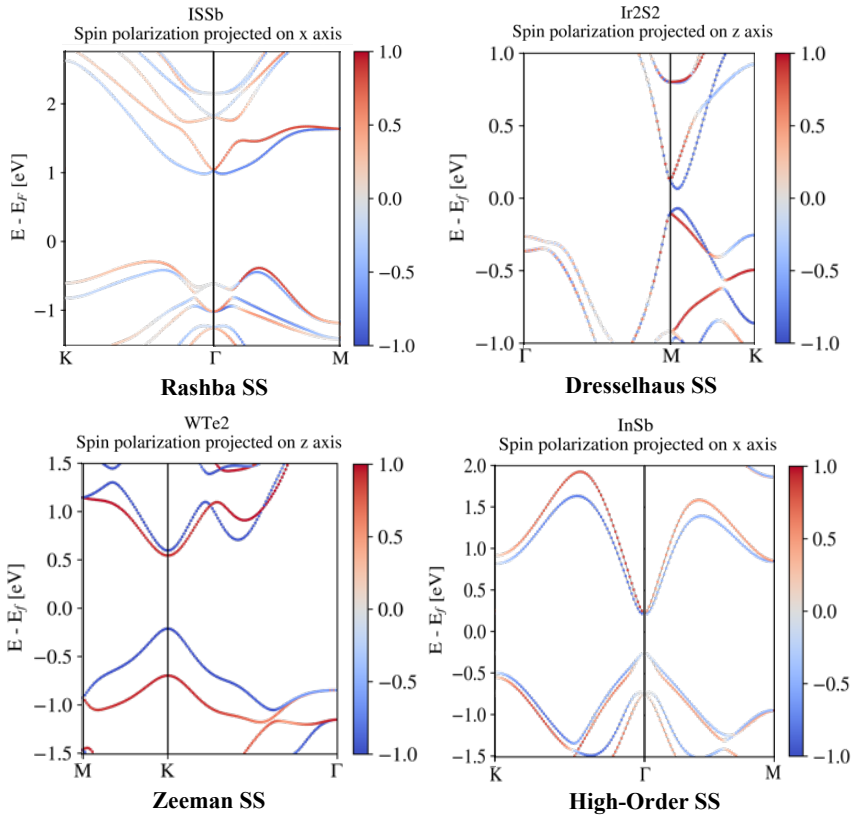

FIG. 4. **Examples of SS identified in the algorithm.** Fragments of band structures represented with spin resolution, classified among the different SS prototypes. The title of each figure represents the chemical formula of the corresponding material and the direction of polarization projection applied to plot the spin texture.

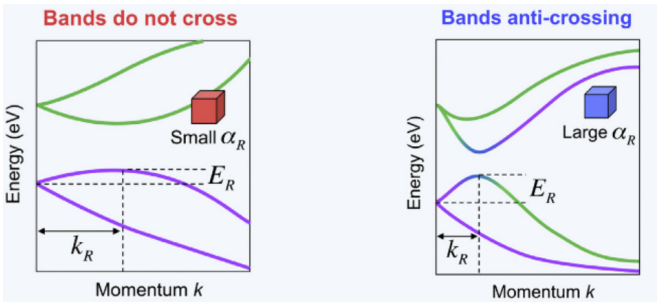

FIG. 5. **Relationship between large Rashba coefficient and anti-crossing bands.** Tight binding model of band structures representing the Rashba SS effect, where bands do not cross (left) and have anti-crossing (right). Purple (green) color represents bands with major contribution from s (p_x) orbitals. As it can be seen, anti-crossing highly contributes to a large Rashba coefficient, where the energy difference is higher while the wavevectors displacement is shorter. Figure extracted from ref [58].

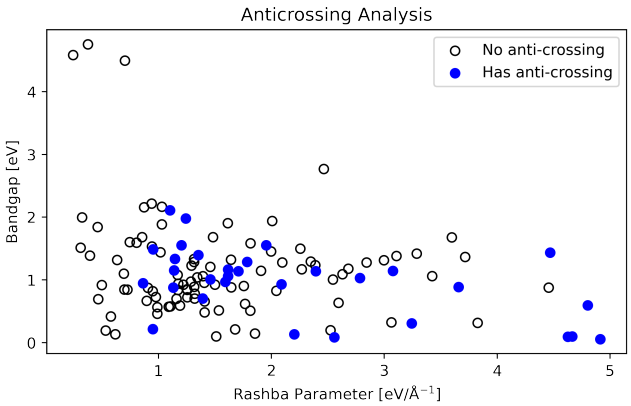

FIG. 6. Distribution of the 124 compounds with Rashba or Dresselhaus SS prototypes identified in this work, according to its SS coefficient $\alpha_{R,D}$ (Rashba parameter in the plot) and its band gap. Filled blue (unfilled black) dots correspond to compounds whose SS was identified to have (do not have) the presence of anti-crossing among valence and conduction bands.

constructed [55], within the Materials Cloud infrastructure [7], to host all these work's results and generated data. There, the reader may find a detailed guide for accessing and opening all the data formats (represented

by the `README.md` file in the repository).

For visual information about individual materials, all calculated band structures, with all projections of spin polarization, are available in specific directories of this repository. They are also followed by `.cif` files, that fully determine the material's structure, as well as rendered images for its illustrative representation. The reader can, therefore, have a correspondence between the SS information found in the SS tables and the actual materials that host them, as well as the location where the specific SSs happen in the system's band structure.

Regarding the raw results of the calculations employed in the computational workflow in this work, these are available in agnostic formats, based on Pymatgen [46] and ASE [52] objects, that do not depend on the DFT code used. This enables the reader to have access to the extensive information about the k-points sampled in reciprocal space for each compound, its calculated eigenvalues, orbital projections, spin polarization expected values, and other relevant information regarding all calculations performed in this work.

Moreover, all the data associated with the provenance of the calculations (e.g. main input and output files) are stored in a separate NOMAD repository [59], openly available online. This ensures the full reproducibility of this work's findings, once every single calculation can be tracked and reproduced with the available information.

Finally, the main results of this work are composed of the post-processed data generated from the developed algorithm for SS identification. For this large amount of information to be available in its full capacity for other large-scale approaches of materials selection and design, a computational database, based on the `MongoDB` framework, was constructed to store all the data here generated. Here again, the `README` file available in the Materials Cloud repository of this work contains detailed information about how the data can be accessed. Each entry in this database, therefore, links together all relevant information of a single material here studied, being segmented into i) material-specific data, ii) band structure-specific data, iii) spin-splitting specific data and iv) DFT calculations specific data, as they were already discussed throughout this section.

By incorporating all of it in a single database, the entire data generated in this work can then be queried with high efficiency, being also suited for direct integration with statistical/machine learning models, and new simulation techniques for materials modeling and design. It is believed, therefore, that the infrastructure developed here can support further theoretical investigations and possibly serve as an initial guide for experimental verifications, providing useful information to help to foster and accelerate the development of materials and devices for spintronic applications.

VI. CONCLUSIONS

Computation techniques, mainly under the formalism of Density Functional Theory, are reshaping the way materials are designed for a vast range of applications, with promising possibilities to tackle various challenges our current society faces. When coupled with the ever-increasing power of high-performance computing resources and robust frameworks for handling calculations, the high-throughput efforts emergent from this combination may be one of the most efficient approaches to explore the vast range of the materials landscape yet to be known.

The data generated by those approaches, due to their digital and structured nature, are also supporting the unfolding and growth of extensive computational databases that gather and curate an enormous amount of materials' information. In this way, they foster an entirely new range of computational approaches that aim at exploring these data, finding trends, and determining guiding directions for to rationalized approach for materials modeling and design.

In this perspective, the work presented here identifies a latent area of research where these large-scale computational efforts can be applied to help accelerate the development of technological devices, targeted at addressing some of the current challenges in our current silicon-based society. After more than five decades of development, the constant advances and miniaturization of electronics, governed by Moore's law, are reaching their physical limits. Moreover, our computer-intensive economy is imposing relevant concerns on the impact of this technology on global energy consumption.

Over time, then, the idea of introducing non-traditional materials and technologies to these applications is gaining traction as one of the promising approaches to keep the scaling of computational power while possibly introducing less energy-intensive ways of manipulating digital information. The field of spintronics then emerges from this perspective as an approach to looking for answers in the space of the electron's spin degrees of freedom, which could physically be accessed by exploring the so-called spin-splitting effects displayed in special classes of materials.

From this perspective, the current work is an important effort in identifying materials with these specific functionalities. We have started from the theoretical foundations and models of spin-splitting effects as the physical guidelines for this search, and encapsulated this knowledge in computationally robust algorithms capable of automatically identifying and classifying these physical effects in a vast range of two-dimensional compounds. With the extensive results and data from the measurements performed for hundreds of materials, we can then construct a novel computational database of spin-splittings in two-dimensional systems.

This database, being openly available, is now part of the vast range of information that composes the founda-

tions of the field of Materials Informatics. By providing extensive information on spin-splittings effects for hundreds of materials, we believe that the availability of such data for the entire research field may serve as an additional reference point for further experimental investigation of previously unrealized compounds.

Moreover, once viewed from above, the data here publish may share hidden trends that connect properties of compounds across the entire materials landscape with the target functionalities of interest. These functionalities, being here the spin-splitting properties of the compounds, have quantifiable metrics that are correlated with the feasibility of real applications in spintronic devices. Understanding how these metrics are interconnected and the factors which play a large influence over them is therefore desirable for a rational design of optimal materials for such applications. Therefore, in addition to the results here shown, we have published a work in the Journal *Nature Scientific Data* that shows how these trends can be explored, using statistical models, to guide the generation of new materials with optimized values for its SS metrics [60].

Naturally, these trends may also represent a deeper and latent knowledge towards the mechanisms at play for spin-splitting effects. In this perspective, the data here available can also serve as a foundation to further theoretical works that aim to understand this complex interplay of materials properties and functionalities, possibly providing new insights into not only the description of those effects but also how they could be controlled in the desirable ways for such device applications.

Finally, the tools, algorithms, and concepts here developed are compatible with new efforts for materials design at a large scale. Our computational code, openly available online, can further be employed in new efforts for the high-throughput study of SS effects in other classes of materials, in addition to providing new tools for the automatic handling of band structures with spin texture resolution. Moreover, the philosophy of the methods here employed, based on the inverse design of materials starting from design principles to the escalation to high-throughput calculations, can be extended straightforwardly to a wide range of different properties of interest, potentially addressing other technological challenges of the society of our time.

Appendix A: DFT

This section aims at introducing some of the central concepts which compose the theoretical basis of some of the main computational methods in the field of quantum materials modeling based on Density Functional Theory (DFT). In this sense, a more detailed and extensive description of the theoretical formalism and computational implementation behind these concepts can be found in the books by Giustino [61] and Martin [62].

1. Foundations of Density Functional Theory

When working with nanomaterials, the phenomena and effects that need to be described to correctly characterize their properties and functionalities are of the order of nanometers (10^{-9} m) or Angstroms (10^{-10} m). On such scale, any classical description of the behavior of continuum matter might fail and the understanding of matter under such circumstances must come within the framework of Quantum Mechanics, where the wavefunction (ψ) associated with the particles, e.g. electrons, plays the major role in the system and thus in its properties.

Considering stationary electronic states, a multi-electronic system, such as the ones we have interest in describing, has in this way a many-body wavefunction (Ψ) associated with it that must obey the time-independent Schrödinger equation:

$$H\Psi = E\Psi, \tag{A1}$$

where H is the Hamiltonian of the system, taking into account the kinetic and potential energies associated with its particles and operates on the wavefunction. The functions, which are eigenfunctions of this operator, represent the possible states of the system and its eigenvalues correspond to the energy associated with such states. The many-body wavefunction which comes out of this equation can describe all the properties associated with the system in consideration, and in this case, where time evolution is not considered, this function depends on the position of each particle, i.e. all the N electrons and M nuclei of the system:

$$\Psi = \Psi(\mathbf{r}_1, \mathbf{r}_2, ..., \mathbf{r}_N, \mathbf{R}_1, \mathbf{R}_2, ..., \mathbf{R}_M), \tag{A2}$$

where $\mathbf{r}$ and $\mathbf{R}$ are taken to be the coordinates of each electron and nucleus in the three-dimensional space.

As the Hamiltonian, being the operator which acts upon the wavefunction, may include all the contributions to the kinetic and potential energy in the system, it can initially be split into terms that take into account different kinds of interactions among the particles of the system:

For the kinetic terms we have:

$$\underbrace{-\sum_{i=1}^{N} \frac{\hbar^2}{2m_e}\nabla_i^2}_{\text{electrons}} \underbrace{-\sum_{I=1}^{M} \frac{\hbar^2}{2M_I}\nabla_I^2}_{\text{nuclei}}. \tag{A3}$$

And for the interactions that contribute to the potential energy:

$$\underbrace{\frac{1}{2}\sum_{i\neq j}\frac{e^2}{4\pi\epsilon_0}\frac{1}{|\mathbf{r}_i-\mathbf{r}_j|}}_{\text{electron-electron interaction}} + \underbrace{\frac{1}{2}\sum_{i\neq j}\frac{e^2}{4\pi\epsilon_0}\frac{Z_I Z_J}{|\mathbf{R}_I-\mathbf{R}_J|}}_{\text{nucleus-nucleus interaction}} - \underbrace{\frac{1}{2}\sum_{i,I}\frac{e^2}{4\pi\epsilon_0}\frac{Z_I}{|\mathbf{r}_i-\mathbf{R}_I|}}_{\text{electron-nucleus interaction}}, \quad \text{(A4)}$$

where i, j run over 1 to N (the number of electrons in the system), and I, J run over 1 to M (number of nuclei). Therefore, the complete many-body time-independent Schrödinger equation can be written as:

$$\left[-\sum_{i=1}^{N}\frac{\hbar^2}{2m_e}\nabla_i^2 - \sum_{I=1}^{M}\frac{\hbar^2}{2M_I}\nabla_I^2 + \frac{1}{2}\sum_{i\neq j}\frac{e^2}{4\pi\epsilon_0}\frac{1}{|\mathbf{r}_i-\mathbf{r}_j|} + \frac{1}{2}\sum_{i\neq j}\frac{e^2}{4\pi\epsilon_0}\frac{Z_I Z_J}{|\mathbf{R}_I-\mathbf{R}_J|} - \frac{1}{2}\sum_{i,I}\frac{e^2}{4\pi\epsilon_0}\frac{Z_I}{|\mathbf{r}_i-\mathbf{R}_I|}\right]\Psi = E\Psi. \quad \text{(A5)}$$

The main problem with this approach to determining the ground state of a quantum system from its many-body wavefunctions is the complexity. There are only analytical solutions for such equations for systems containing a single electron, e.g. the Hydrogen atom, and numerical approaches are infeasible for systems larger than small molecules. Given the fact that the many-body wavefunction is a function dependent on the spatial coordinates of each particle in the system, discretizing the problem into a uniform mesh of points to solve by linear methods would result in an incredibly large array of data, even for simple systems like silicon (with only two atoms in the unit cell), making it infeasible for computational implementations.

One direct approach to simplify such a complex problem is to take into consideration that the mass of nuclei is much larger than the mass of electrons, and thus the wavelength associated with them should be much smaller, and negligible in this sense. Moreover, for the study of solids and molecules, one can consider that such nuclei should remain fixed at their positions, once their equilibrium state is determined. Such claims form the base ideas of the Born-Oppenheimer approximation, which is able to usually reproduce appropriate results for a large number of different systems in condensed matter. Therefore, when removing the nuclei kinetic energy term, considering the nucleus-nucleus interaction a constant, equation A5 turns into (considering atomic units for simplicity of notation):

$$\left[-\sum_i\frac{1}{2}\nabla_i^2 - \sum_i\sum_I\frac{Z_I}{|\mathbf{r}_i-\mathbf{R}_I|} + \frac{1}{2}\sum_{i\neq j}\frac{1}{|\mathbf{r}_i-\mathbf{r}_j|}\right]\Psi = E\Psi. \quad \text{(A6)}$$

However, only this simplification is not enough to make the problem directly soluble in most cases. The grand success in Density Functional Theory is based on a larger shift, that considers the electronic density of the ground state $n(\mathbf{r})$ as the central quantity to describe the quantum system, instead its many-body wavefunction $\Psi(\mathbf{r}_1...\mathbf{r}_N)$. This concept was first introduced by the consideration that, for any quantum system, the external potential and the number of electrons uniquely determine its charge density. From that, the first Hohenberg-Kohn theorem [63] demonstrated that the inverse is also true:

> **HK 1:** *In the ground state, the charge density $n(\mathbf{r})$ determines uniquely, i.e. in a one-to-one correspondence, the external potential and the number of electrons.*

In this perspective, $n(\mathbf{r})$ (from the ground state) determines the external potential V_{ext} that enters the many-body Schrödinger equation. This in turn could be used to solve for the ground-state wavefunctions Ψ, which determine, for any quantum system, the total ground state energy E. The problem is then fully characterized by $n(\mathbf{r})$, and a well define route exists connecting $n(\mathbf{r})$ to V_{ext}, that leads to $\hat{H}$ and then be solved to yield Ψ and then E. This ultimately means that both Ψ and E are *functionals* of $n(\mathbf{r})$. This last functional of the charge density $E = F[n(\mathbf{r})]$ is commonly defined (symbolically until now) as:

$$F[n(\mathbf{r})] = \langle\Psi|\hat{T}+\hat{V}_{e-e}|\Psi\rangle + \int n(\mathbf{r})V_{ext}(\mathbf{r})d\mathbf{r}, \quad \text{(A7)}$$

where $\hat{T}$ represents the total kinetic energy operator while $\hat{V}_{e-e}$ accounts for the (many-body) electron-electron interactions.

At first, we know that the connection from $n(\mathbf{r})$ to E exists, but until then no useful way of computing it was devised. The second Hohenberg-Kohn theorem [63] then comes to shine some light on this problem using the variational principle, that is:

> **HK 2:** *The ground state energy can be obtained variationally: the density that minimizes the total energy is the exact ground state density.*

By this principle, the minimum value for the functional $F[n]$ is obtained when infinitesimal perturbations in $n(\mathbf{r})$ do not change its value. In short, this is expressed by its derivative functional:

$$\left.\frac{\delta F[n]}{\delta n}\right|_{n0} = 0, \tag{A8}$$

at the ground state charge density n_0.

However, the direct evaluation of $F[n]$ still requires the solution of the many-body Schrödinger equation. Despite being exact, this formalism until here would be of no help, from the fact that it still requires the solution of the very problem we were trying to avoid. To bypass this, the auxiliary Kohn-Sham (KS) system was then introduced [64]. It consists of a system of *non-interacting particles* that have a unique mapping to the ground state charge density of the many-body problem. In order to accomplish this, these KS single-body states live in an effective potential (the KS potential) such as the charge density produced by them is identical to the true physical system.

In this auxiliary non-interacting system, its energy terms, namely $\hat{T}$ and $\hat{V}_{e-e}$, are better defined, resulting in a more explicit version of the energy functional in terms of the Kohn-Sham wavefunctions ϕ_i:

$$E[\{\phi_i\}] = \sum_{i=1}^{N} -\frac{1}{2}\int \phi_i^*(\mathbf{r})\nabla^2\phi_i(\mathbf{r})d\mathbf{r} + E_H[n(\mathbf{r})] + E_{xc}[n(\mathbf{r})] + \int V_{ext}(\mathbf{r})n(\mathbf{r})d\mathbf{r}, \tag{A9}$$

where $E_H[n(\mathbf{r})]$ stands for the Hartree energy, which accounts for the electrostatic interaction of the KS-particle with the "electronic" cloud formed by the other particles, and has the explicit form:

$$E_H[n(\mathbf{r})] = \frac{1}{2}\iint \frac{n(\mathbf{r}_1)n(\mathbf{r}_2)}{|\mathbf{r}_1 - \mathbf{r}_2|}d\mathbf{r}_1 d\mathbf{r}_2. \tag{A10}$$

The exact therm for $E_{xc}[n(\mathbf{r})]$ in its closed form, on the other hand, remains to this date unknown. Being coined as the *Exchange-correlation* part, it encapsulates all our approximations for the additional terms that would correct the charge density of the non-interacting system to reproduce the many-body problem (beyond accounting for exchange and correlation effects, per se, this therm would in fact also be responsible for correcting the kinetic energies of the single-body states to account for the *interacting* system). We note here that the specific parameterizations for E_{xc} are an area of research itself, and extensively characterizing the different approaches proposed for it are beyond the scope of this section (refs. [62, 65] present interesting discussions about the topic).

Moreover, for a non-interacting system, a Slater determinant of single-particle states is its exact solution (in addition to correctly addressing the anti-symmetry of the wavefunctions in such a fermionic system). By also requiring these KS wavefunctions to be orthogonal to each other, we have:

$$\int \phi_i^*(\mathbf{r})\phi_j(\mathbf{r})d\mathbf{r} = \delta_{ij}. \tag{A11}$$

In this perspective, it can be shown [61] that the minimization of the energy functional E from equation A9, with respect to variations of the functions ϕ_i in the form of a Slater determinant, with the additional requirement of orthogonality from equation A11, produces the so-called *Kohn-Sham equations*:

$$\left[-\frac{1}{2}\nabla^2 + v_H(\mathbf{r}) + v_{xc}(\mathbf{r}) + v_{ext}(\mathbf{r})\right]\phi_i = \epsilon_i\phi_i(\mathbf{r}), \tag{A12}$$

where:

$$v_H(\mathbf{r}) = \int \frac{n(\mathbf{r})}{|\mathbf{r} - \mathbf{r}'|}d\mathbf{r}', \tag{A13}$$

$$v_{xc}(\mathbf{r}) = \frac{\delta E_{xc}}{\delta n(\mathbf{r})}. \tag{A14}$$

The ground state charge density can be therefore computed from the single-particle wavefunctions directly:

$$n(\mathbf{r}) = \sum_{i=1}^{N} |\phi_i(\mathbf{r})|^2. \tag{A15}$$

Therefore, determining the one particle wavefunctions can be done with the use of equation A12, where v_H is determined by equation A13 and v_{xc} can be quantified from A14 once a specific parameterization for E_{xc} is employed. However, as it can be seen, the Hartree and exchange-correlation potentials have both a dependence upon the charge density, which in its turn is dependent upon the single particle wavefunction itself (through eq. A15). Therefore the method for solving such a system of equations is based on what is called a *self-consistent loop*: given a set of atomic coordinates, an initial charge density is estimated at the beginning of the calculation, e.g. by the overlap of atomic orbitals, and used to compute the different potential terms. Once v_H, v_{xc} and v_{ext} is evaluated, it can be used into the Kohn-Sham equation (A12) to determine the single particle wavefunctions ϕ_i and its eigenvalues ϵ_i. The charge density is then reconstructed using eq. A15 with the N single-particle wavefunctions with the lowest eigenvalues. The procedure is then repeated until self-consistency is achieved: the charge density does not change within a given tolerance throughout the loop of evaluations, and then the calculation, more precisely its charge density, is considered to be *converged*. From this point, once the ground state charge density $n(\mathbf{r})$ is determined, the total energy of the system can be computed from equation A9.

2. DFT implemented to crystalline systems

Crystals are the classes of materials with long-range order: their structure can be defined by an atomic group, usually called *basis*, arranged in a 3D cell that is periodic repeated. In this context, one can deduce an alternative form for the Kohn-Sham equations from the last section to account for the periodic conditions that are suited to describe crystalline materials.

In such periodic systems, it follows that its Hamiltonian is also periodic, i.e. it must be invariant under a spacial translation operator $\hat{T}_{\mathbf{R}}$ which follows the symmetry of the crystal. It is expected once all translations along the vector given by $\mathbf{R} = l\mathbf{a_1} + m\mathbf{a_2} + l\mathbf{a_3}$ (where a_i are lattice vectors of the crystal and l, n, m integers) map the system onto itself (because of periodic conditions). In short, the invariance of $\hat{H}$ with respect to $\hat{T}_{\mathbf{R}}$ is encapsulated by the commutation relation:

$$[\hat{H}, \hat{T}_{\mathbf{R}}] = 0. \tag{A16}$$

In this context, the *Bloch theorem* shows that, for any system that follows the symmetry relation expressed in eq. A16, it follows that its single-particle electronic wavefunctions can be expressed as [66]:

$$\phi_i \to \phi_{i\mathbf{k}}(\mathbf{r}) = e^{i\mathbf{k}\cdot\mathbf{r}} u_{i\mathbf{k}}(\mathbf{r}), \tag{A17}$$

where $u_{i\mathbf{k}}(\mathbf{r})$ are functions that follow the periodicity of the crystal, i.e. $u_{i,\mathbf{k}}(\mathbf{r}+\mathbf{T}) = u_{i\mathbf{k}}(\mathbf{r})$ for $\mathbf{T} = l\mathbf{a_1} + m\mathbf{a_2} + l\mathbf{a_3}$. The single-particle wavefunctions now gain an additional quantum number $\mathbf{k}$, which is often associated with the electronic wavevector (its *crystal momentum*).

Substituting the form for $\phi_{i\mathbf{k}}$ from equation A17 into the Kohn-Sham equations in A12, and multiplying both sides by $e^{-i\mathbf{k}\cdot\mathbf{r}}$, we have:

$$-e^{-i\mathbf{k}\cdot\mathbf{r}}\frac{1}{2}\nabla^2[e^{i\mathbf{k}\cdot\mathbf{r}}u_{i\mathbf{k}}(\mathbf{r})] + v_{tot}(\mathbf{r})u_{i\mathbf{k}}(\mathbf{r}) = \epsilon_{i\mathbf{k}}u_{i\mathbf{k}}(\mathbf{r}), \tag{A18}$$

where we have made $v_{tot}(\mathbf{r}) = v_H(\mathbf{r}) + v_{xc}(\mathbf{r}) + v_{ext}(\mathbf{r})$.

The first therm can be directly evaluated to yield:

$$e^{-i\mathbf{k}\cdot\mathbf{r}}\frac{1}{2}\nabla^2[e^{i\mathbf{k}\cdot\mathbf{r}}u_{i\mathbf{k}}(\mathbf{r})] = (\nabla + i\mathbf{k})^2 u_{i\mathbf{k}}(\mathbf{r}), \tag{A19}$$

leading to the *periodic version* of the Kohn-Sham equations:

$$\left[-\frac{1}{2}(\nabla + i\mathbf{k})^2 + v_{tot}(\mathbf{r})\right] u_{i\mathbf{k}}(\mathbf{r}) = \epsilon_{i\mathbf{k}}u_{i\mathbf{k}}(\mathbf{r}). \tag{A20}$$

The problem then reduces to the determination of the lattice periodic function $u_{i\mathbf{k}}(\mathbf{r})$, which is often expanded as a Fourier series of the form:

$$u_{n\mathbf{k}}(\mathbf{r}) = \sum_{\mathbf{G}} c_{n\mathbf{k}}^{\mathbf{G}} e^{i\mathbf{G}\cdot\mathbf{r}}, \tag{A21}$$

(where the sub-index i has been replaced by n here to not get confused with the imaginary number i).

Therefore, the equations for the Kohn-Sham orbitals are ultimately solved by numerically determining the coefficients $c_{n\mathbf{k}}^{\mathbf{G}}$ that diagonalize the equations in A20 for each band indexes i and wavevector $\mathbf{k}$.

[1] K. T. Butler, D. W. Davies, H. Cartwright, O. Isayev, and A. Walsh, Machine learning for molecular and materials science, Nature **559**, 547 (2018).

[2] K. Lejaeghere, G. Bihlmayer, T. Björkman, P. Blaha, S. Blügel, V. Blum, D. Caliste, I. E. Castelli, S. J. Clark, A. Dal Corso, *et al.*, Reproducibility in density functional theory calculations of solids, Science **351** (2016).

[3] G. Prandini, A. Marrazzo, I. E. Castelli, N. Mounet, and N. Marzari, Precision and efficiency in solid-state pseudopotential calculations, npj Computational Materials **4**, 1 (2018).

[4] N. Marzari, A. Ferretti, and C. Wolverton, Electronic-structure methods for materials design, Nature Materials **20**, 736 (2021).

[5] N. Nosengo, The material code: Machine-learning techniques could revolutionize how materials science is done, Nature **533** (2016).

[6] N. Marzari, The frontiers and the challenges, Nature materials **15**, 381 (2016).

[7] L. Talirz, S. Kumbhar, E. Passaro, A. V. Yakutovich, V. Granata, F. Gargiulo, M. Borelli, M. Uhrin, S. P. Huber, S. Zoupanos, C. S. Adorf, C. W. Andersen, O. Schütt, C. A. Pignedoli, D. Passerone, J. VandeVondele, T. C. Schulthess, B. Smit, G. Pizzi, and N. Marzari, Materials cloud, a platform for open computational science, Scientific Data **7**, 10.1038/s41597-020-00637-5 (2020).

[8] A. Jain, S. P. Ong, G. Hautier, W. Chen, W. D. Richards, S. Dacek, S. Cholia, D. Gunter, D. Skinner, G. Ceder, and K. A. Persson, Commentary: The materials project: A materials genome approach to accelerating materials innovation, APL Materials **1**, 011002 (2013).

[9] S. Curtarolo, W. Setyawan, S. Wang, J. Xue, K. Yang, R. H. Taylor, L. J. Nelson, G. L. W. Hart, S. Sanvito, M. Buongiorno-Nardelli, N. Mingo, and O. Levy, Aflowlib.org: A distributed materials properties repository from high-throughput ab initio calculations, Computational Materials Science **58**, 227 (2012).

[10] S. Kirklin, J. E. Saal, B. Meredig, A. Thompson, J. W. Doak, M. Aykol, S. Rühl, and C. Wolverton, The open quantum materials database (oqmd): Assessing the accuracy of dft formation energies, npj Computational Ma-

terials **1**, 10.1038/npjcompumats.2015.10 (2015).
[11] K. Choudhary, K. F. Garrity, A. C. Reid, B. DeCost, A. J. Biacchi, A. R. H. Walker, Z. Trautt, J. Hattrick-Simpers, A. G. Kusne, A. Centrone, *et al.*, Jarvis: An integrated infrastructure for data-driven materials design, arXiv preprint arXiv:2007.01831 (2020).
[12] W. Y. Wang, J. Li, W. Liu, and Z.-K. Liu, Integrated computational materials engineering for advanced materials: A brief review, Computational Materials Science **158**, 42 (2019).
[13] K. S. Novoselov, A. K. Geim, S. V. Morozov, D. Jiang, Y. Zhang, S. V. Dubonos, I. V. Grigorieva, and A. A. Firsov, Electric field in atomically thin carbon films, Science **306**, 666 (2004).
[14] S. Lebègue, T. Björkman, M. Klintenberg, R. M. Nieminen, and O. Eriksson, Two-dimensional materials from data filtering and ab initio calculations, PHYSICAL REVIEW X **3**, 10.1103/PhysRevX.3.031002 (2013).
[15] G. Cheon, K. A. N. Duerloo, A. D. Sendek, C. Porter, Y. Chen, and E. J. Reed, Data mining for new two- and one-dimensional weakly bonded solids and lattice-commensurate heterostructures, Nano Letters **17**, 1915 (2017).
[16] P. M. Larsen, M. Pandey, M. Strange, and K. W. Jacobsen, Definition of a scoring parameter to identify low-dimensional materials components, Phys. Rev. Materials **3**, 034003 (2019).
[17] P. Gorai, E. S. Toberer, and V. Stevanovic, Computational identification of promising thermoelectric materials among known quasi-2d binary compounds, Journal of Materials Chemistry A **4**, 11110 (2016).
[18] H. Gao, J. Wang, Z. Guo, and J. Sun, Dimensionalities and multiplicities determination of crystal nets, npj Computational Materials 2020 6:1 **6**, 1 (2020).
[19] G. Pizzi, A. Cepellotti, R. Sabatini, N. Marzari, and B. Kozinsky, Aiida: automated interactive infrastructure and database for computational science, Computational Materials Science **111**, 218 (2016).
[20] S. P. Huber, S. Zoupanos, M. Uhrin, L. Talirz, L. Kahle, R. Häuselmann, D. Gresch, T. Müller, A. V. Yakutovich, C. W. Andersen, F. F. Ramirez, C. S. Adorf, F. Gargiulo, S. Kumbhar, E. Passaro, C. Johnston, A. Merkys, A. Cepellotti, N. Mounet, N. Marzari, B. Kozinsky, and G. Pizzi, Aiida 1.0, a scalable computational infrastructure for automated reproducible workflows and data provenance, Scientific Data **7**, 1 (2020).
[21] N. Mounet, M. Gibertini, P. Schwaller, D. Campi, A. Merkys, A. Marrazzo, T. Sohier, I. E. Castelli, A. Cepellotti, G. Pizzi, and N. Marzari, Two-dimensional materials from high-throughput computational exfoliation of experimentally known compounds, Nature Nanotechnology **13**, 246 (2018).
[22] O. I. Malyi, K. V. Sopiha, and C. Persson, Energy, phonon, and dynamic stability criteria of two-dimensional materials (2019).
[23] N. Mounet, M. Gibertini, P. Schwaller, D. Campi, A. Merkys, A. Marrazzo, T. Sohier, I. E. Castelli, A. Cepellotti, G. Pizzi, and N. Marzari, Two-dimensional materials from high-throughput computational exfoliation of experimentally known compounds (data download), Materials Cloud Achive **2017.0008/v1**, 10.24435/materialscloud:2017.0008/v1 (2017).
[24] S. Haastrup, M. Strange, M. Pandey, T. Deilmann, P. S. Schmidt, N. F. Hinsche, M. N. Gjerding, D. Torelli, P. M. Larsen, A. C. Riis-Jensen, J. Gath, K. W. Jacobsen, J. J. Mortensen, T. Olsen, and K. S. Thygesen, The computational 2d materials database: High-throughput modeling and discovery of atomically thin crystals, 2D Materials **5**, 10.1088/2053-1583/aacfc1 (2018).
[25] J. Zhou, L. Shen, M. D. Costa, K. A. Persson, S. P. Ong, P. Huck, Y. Lu, X. Ma, Y. Chen, H. Tang, and Y. P. Feng, 2dmatpedia, an open computational database of two-dimensional materials from top-down and bottom-up approaches, Scientific data **6**, 86 (2019).
[26] E. S. Penev, N. Marzari, and B. I. Yakobson, Theoretical prediction of two-dimensional materials, behavior, and properties, ACS nano **15**, 5959 (2021).
[27] G. R. Schleder, C. M. Acosta, and A. Fazzio, Exploring two-dimensional materials thermodynamic stability via machine learning, ACS applied materials & interfaces **12**, 20149 (2019).
[28] M. C. Sorkun, S. Astruc, J. V. A. Koelman, and S. Er, An artificial intelligence-aided virtual screening recipe for two-dimensional materials discovery, npj Computational Materials **6**, 1 (2020).
[29] K. Khan, A. K. Tareen, M. Aslam, R. Wang, Y. Zhang, A. Mahmood, Z. Ouyang, H. Zhang, and Z. Guo, Recent developments in emerging two-dimensional materials and their applications, Journal of Materials Chemistry C **8**, 387 (2020).
[30] K. S. Novoselov, A. Mishchenko, A. Carvalho, and A. H. C. Neto, 2d materials and van der waals heterostructures, Science **353**, 10.1126/science.aac9439 (2016).
[31] F. Pulizzi, Spintronics, Nature materials **11**, 367 (2012).
[32] I. Žutić, J. Fabian, and S. Das Sarma, Spintronics: Fundamentals and applications, Rev. Mod. Phys. **76**, 323 (2004).
[33] C. M. Acosta and A. Fazzio, Spin-polarization control driven by a rashba-type effect breaking the mirror symmetry in two-dimensional dual topological insulators, Phys. Rev. Lett. **122**, 036401 (2019).
[34] M. Gmitra and J. Fabian, Proximity effects in bilayer graphene on monolayer wse_2: Field-effect spin valley locking, spin-orbit valve, and spin transistor, Phys. Rev. Lett. **119**, 146401 (2017).
[35] C. M. Acosta, A. Fazzio, and G. M. Dalpian, Zeeman-type spin splitting in nonmagnetic three-dimensional compounds, npj Quantum Materials **4**, 1 (2019).
[36] C. Cohen-Tannoudji, B. Diu, and F. Laloe, Quantum mechanics, volume 2, Quantum Mechanics **2**, 626 (1986).
[37] A. Manchon, H. C. Koo, J. Nitta, S. Frolov, and R. Duine, New perspectives for rashba spin–orbit coupling, Nature materials **14**, 871 (2015).
[38] P. Zeeman, The effect of magnetisation on the nature of light emitted by a substance, nature **55**, 347 (1897).
[39] Y. Li, J. Ludwig, T. Low, A. Chernikov, X. Cui, G. Arefe, Y. D. Kim, A. M. Van Der Zande, A. Rigosi, H. M. Hill, *et al.*, Valley splitting and polarization by the zeeman effect in monolayer $mose_2$, Physical review letters **113**, 266804 (2014).
[40] E. Rashba, Properties of semiconductors with an extremum loop. i. cyclotron and combinational resonance in a magnetic field perpendicular to the plane of the loop, Sov. Phys.-Solid State **2**, 1109 (1960).
[41] Y. A. Bychkov and É. I. Rashba, Properties of a 2d electron gas with lifted spectral degeneracy, JETP lett **39**,

78 (1984).
[42] A. Manchon, H. C. Koo, J. Nitta, S. M. Frolov, and R. A. Duine, New perspectives for rashba spin-orbit coupling, Nature Materials **14**, 871 (2015).
[43] G. Dresselhaus, Spin-orbit coupling effects in zinc blende structures, Phys. Rev. **100**, 580 (1955).
[44] S. Haastrup, M. Strange, M. Pandey, T. Deilmann, P. S. Schmidt, N. F. Hinsche, M. N. Gjerding, D. Torelli, P. M. Larsen, A. C. Riis-Jensen, J. Gath, K. W. Jacobsen, J. J. Mortensen, T. Olsen, and K. S. Thygesen, The computational 2d materials database: high-throughput modeling and discovery of atomically thin crystals, 2D Materials **5**, 042002 (2018).
[45] P. M. Larsen, M. Pandey, M. Strange, and K. W. Jacobsen, Definition of a scoring parameter to identify low-dimensional materials components, Phys. Rev. Materials **3**, 034003 (2019).
[46] S. P. Ong, W. D. Richards, A. Jain, G. Hautier, M. Kocher, S. Cholia, D. Gunter, V. L. Chevrier, K. A. Persson, and G. Ceder, Python materials genomics (pymatgen): A robust, open-source python library for materials analysis, Computational Materials Science **68**, 314 (2013).
[47] G. Kresse and J. Furthmüller, Efficient iterative schemes for ab initio total-energy calculations using a plane-wave basis set, Physical review B **54**, 11169 (1996).
[48] G. Kresse and J. Furthmüller, Efficiency of ab-initio total energy calculations for metals and semiconductors using a plane-wave basis set, Computational materials science **6**, 15 (1996).
[49] G. Kresse and J. Hafner, Ab initio molecular dynamics for liquid metals, Physical review B **47**, 558 (1993).
[50] J. P. Perdew, K. Burke, and M. Ernzerhof, Generalized gradient approximation made simple, Phys. Rev. Lett. **77**, 3865 (1996).
[51] A. Jain, S. P. Ong, G. Hautier, W. Chen, W. D. Richards, S. Dacek, S. Cholia, D. Gunter, D. Skinner, G. Ceder, and K. A. Persson, Commentary: The materials project: A materials genome approach to accelerating materials innovation, APL Materials **1**, 011002 (2013).
[52] A. H. Larsen, J. J. Mortensen, J. Blomqvist, I. E. Castelli, R. Christensen, M. Dułak, J. Friis, M. N. Groves, B. Hammer, C. Hargus, E. D. Hermes, P. C. Jennings, P. B. Jensen, J. Kermode, J. R. Kitchin, E. L. Kolsbjerg, J. Kubal, K. Kaasbjerg, S. Lysgaard, J. B. Maronsson, T. Maxson, T. Olsen, L. Pastewka, A. Peterson, C. Rostgaard, J. Schiøtz, O. Schütt, M. Strange, K. S. Thygesen, T. Vegge, L. Vilhelmsen, M. Walter, Z. Zeng, and K. W. Jacobsen, The atomic simulation environment—a python library for working with atoms, Journal of Physics: Condensed Matter **29**, 273002 (2017).
[53] H. J. Monkhorst and J. D. Pack, Special points for brillouin-zone integrations, Phys. Rev. B **13**, 5188 (1976).
[54] P. Wisesa, K. A. McGill, and T. Mueller, Efficient generation of generalized monkhorst-pack grids through the use of informatics, Phys. Rev. B **93**, 155109 (2016).
[55] G. M. Nascimento, E. Ogoshi, A. Fazzio, C. M. Acosta, and G. M. Dalpian, High throughput inverse design and bayesian optimization of functionalities: spin splitting in two-dimensional compounds, Materials Cloud Archive **2021.224**, 10.24435/materialscloud:kr-7s (2021).
[56] H. Yuan, M. S. Bahramy, K. Morimoto, S. Wu, K. Nomura, B.-J. Yang, H. Shimotani, R. Suzuki, M. Toh, C. Kloc, *et al.*, Zeeman-type spin splitting controlled by an electric field, Nature Physics **9**, 563 (2013).
[57] D. Xiao, G.-B. Liu, W. Feng, X. Xu, and W. Yao, Coupled spin and valley physics in monolayers of mos 2 and other group-vi dichalcogenides, Physical review letters **108**, 196802 (2012).
[58] C. M. Acosta, E. Ogoshi, A. Fazzio, G. M. Dalpian, and A. Zunger, The rashba scale: Emergence of band anticrossing as a design principle for materials with large rashba coefficient, Matter **3**, 145 (2020).
[59] G. M. Nascimento, E. Ogoshi, A. Fazzio, C. M. Acosta, and G. M. Dalpian, 2d ss materials, NOMAD https://dx.doi.org/10.17172/NOMAD/2021.09.20-2 (2021).
[60] G. M. Nascimento, E. Ogoshi, A. Fazzio, C. M. Acosta, and G. M. Dalpian, High-throughput inverse design and bayesian optimization of functionalities: spin splitting in two-dimensional compounds, Scientific data **9**, 1 (2022).
[61] F. Giustino, *Materials Modelling using Density Functional Theory* (Oxford University Press, 2014) p. 286.
[62] R. M. Martin, *Electronic structure : basic theory and practical methods* (Cambridge University Press, 2008) p. 624.
[63] P. Hohenberg and W. Kohn, Inhomogeneous electron gas, Phys. Rev. **136**, B864 (1964).
[64] W. Kohn and L. J. Sham, Self-consistent equations including exchange and correlation effects, Phys. Rev. **140**, A1133 (1965).
[65] J. Kohanoff, *Electronic structure calculations for solids and molecules: theory and computational methods* (Cambridge university press., 2006).
[66] F. Bloch, Über die quantenmechanik der elektronen in kristallgittern, Zeitschrift für physik **52**, 555 (1929).

Appendix B: SS Tables

Rashba SS Materials

Table B1. List of Rashba SS prototypes identified in the valence (V) and/or conduction (C) bands for materials with polar structure. Each material is presented as a combination of chemical formula and ending with its respective ID from the C2DB Database [1]. *SG index* represents the space group symbol (number) of the material's structure according to the precision criteria employed in this work for symmetry identification. ΔE_{hull} is the energy above convex hull reported by the C2DB database. *Bandgap*, *k-path*, α_R, ΔE_{SS}, $\Delta E_{VBM/CBM}$ and *AC* stand for the energy band gap, k-path between high-symmetry k-points where the SS is identified, Rashba coefficient [eV/Å^{-1}], spin-splitting magnitude, difference in energy between the maximum value of the SS and its respective band edge (VBM or CBM) and the presence of anti-crossing bands, respectively. All energy-related values are in eV.

Entry Info					Spin Splitting Info					
Formula	C2DB ID	SG index	ΔE_{hull}	Bandgap	Band	k-path	α_R	ΔE_{SS}	$\Delta E_{VBM/CBM}$	AC
ISbSe	df0019ec24b5	P3m1 (156)	0.0	1.061	V	M→K	2.431	0.146	0.402	False
					C	Γ→M	1.589	0.156	0.0	True
					C	Γ→K	1.616	0.154	0.0	True
BrSbTe	f1e78a09001d	P3m1 (156)	0.13	1.331	V	M→K	1.315	0.093	0.584	False
BrSbTe	18e62ba75259	P3m1 (156)	0.0	1.089	V	Γ→M	2.631	0.09	0.028	False
					V	Γ→K	2.454	0.108	0.0	False
ClSbSe	f705a30af945	P3m1 (156)	0.146	1.68	V	M→K	1.483	0.118	0.433	False
SSeW	001e03f2c095	P3m1 (156)	0.01	1.417	C	Γ→M	3.284	0.177	0.287	False
					C	Γ→K	3.288	0.214	0.041	False
BiBrTe	f4f45fcade85	P3m1 (156)	0.117	0.916	V	M→K	0.498	0.094	0.7	False
STeW	75ee10091f43	P3m1 (156)	0.086	1.168	C	M→Γ	2.27	0.268	0.188	False
					C	Γ→K	3.947	0.142	0.002	False
MoSTe	2ea941c8bc3c	P3m1 (156)	0.223	0.196	C	M→K	2.358	0.081	0.288	False
					C	Γ→K	2.525	0.224	0.102	False
ISbTe	0f02957b17cf	P3m1 (156)	0.0	0.886	V	Γ→M	3.658	0.076	0.014	True
					V	Γ→K	3.526	0.081	0.0	True
Sn2Te2	03bcf7dcdaf2	$Pmn2_1$(31)	0.063	0.595	C	Y→Γ	4.804	0.081	0.0	True
SeTeW	6e2a4c6f4f57	P3m1 (156)	0.042	1.058	C	M→Γ	1.394	0.182	0.331	False
S2Sn2	7a8373382b33	$Pmn2_1$(31)	0.043	1.434	C	Y→Γ	4.469	0.101	0.0	True
SeSn	d59c96fdfda1	P3m1 (156)	0.098	2.156	V	M→K	0.873	0.113	0.539	False
BiBrS	49b7be14f786	P3m1 (156)	0.0	1.227	C	Γ→M	1.271	0.164	0.0	False
					C	Γ→K	1.293	0.162	0.0	False
AsClTe	fba4cc0df459	P3m1 (156)	0.194	1.316	C	Γ→K	0.634	0.121	0.34	False
ClSbTe	04fdd7d1ec5c	P3m1 (156)	0.153	1.439	V	M→K	1.018	0.15	0.609	False
					C	M→Γ	0.711	0.114	0.081	False
BiBrSe	de5756e4fbfa	P3m1 (156)	0.0	1.03	V	Γ→M	2.784	0.08	0.022	True
					V	Γ→K	2.634	0.082	0.0	True
					C	Γ→M	1.366	0.14	0.0	True
					C	Γ→K	1.417	0.137	0.0	True
Bi2P2S6	287dcf4f1a19	P1 (1)	0.053	0.953	C	Γ→Y	0.795	0.176	0.0	False
					C	Y→Γ	1.406	0.183	0.0	False
					C	Y→H	1.248	0.245	0.133	False
					C	C→H	0.491	0.245	0.133	False
					C	Γ→X	0.882	0.112	0.022	False
BiClS	99fd027b1d0b	P3m1 (156)	0.12	1.841	C	M→Γ	0.461	0.224	0.231	False
AsBrS	1dcd471c2288	P3m1 (156)	0.034	1.38	V	M→K	3.109	0.125	0.497	False
STeW	916afba26723	P3m1 (156)	0.266	0.191	C	M→Γ	3.622	0.158	0.262	False
					C	M→K	3.414	0.266	0.281	False
					C	Γ→K	0.533	0.118	0.619	False
BiClTe	968a6902b7f5	P3m1 (156)	0.0	0.938	V	M→K	1.175	0.208	0.587	False
					C	M→K	0.992	0.113	1.155	False
AsBrTe	671e6de2497a	P3m1 (156)	0.163	1.098	C	Γ→M	0.694	0.079	0.297	False
					C	Γ→K	0.618	0.142	0.31	False
AsISe	5d829e480507	P3m1 (156)	0.0	1.164	V	M→K	1.626	0.153	0.516	False

Entry Info					Spin Splitting Info					
Formula	C2DB ID	SG index	ΔE_{hull}	Bandgap	Band	k-path	α_R	ΔE_{SS}	$\Delta E_{VBM/CBM}$	AC
					C	Γ→M	1.583	0.116	0.0	False
					C	Γ→K	1.615	0.113	0.0	True
ClSbSe	0c0fbdaf8f4a	P3m1 (156)	0.014	1.177	V	Γ→M	2.682	0.093	0.035	False
					V	Γ→K	2.448	0.094	0.0	False
ClSbTe	da5fd2bb47af	P3m1 (156)	0.008	1.291	V	M→Γ	2.891	0.127	0.034	False
					V	M→K	2.35	0.149	0.324	False
Cr2W2Te8	62bb754c4cb2	Pm (6)	0.082	0.512	V	Γ→X	1.535	0.211	0.0	False
					V	Y→S	1.105	0.207	0.369	False
					V	Γ→S	0.686	0.13	0.16	False
Mo2W2Se8	a1d716aad84d	P1 (1)	0.0	1.288	V	X→Γ	1.784	0.313	0.0	True
BiITe	2d41b3dd1772	P3m1 (156)	0.0	0.701	C	Γ→M	2.065	0.128	0.0	False
					C	M→K	1.391	0.137	1.113	True
					C	Γ→K	2.086	0.127	0.0	False
ZrTi3Se8	52a5e2b280d4	P1 (1)	0.131	0.571	V	S→Y	1.091	0.088	0.042	False
					V	S→Γ	0.48	0.102	0.04	False
BiBrSe	11db0908d9ef	P3m1 (156)	0.111	1.385	C	M→Γ	0.393	0.2	0.413	False
P2Sb2Te6	82b85dfd7723	P1 (1)	0.14	0.633	V	Y→Γ	2.466	0.226	0.007	False
					V	X→Γ	2.596	0.223	0.0	False
					C	Y→Γ	1.057	0.135	0.0	False
					C	X→Γ	0.92	0.134	0.002	False
WCr3S8	dc4259e69783	Pmm2 (25)	0.009	0.887	V	X→Γ	1.317	0.119	0.0	False
Cr2Mo2Te8	988b11badabb	P1 (1)	0.067	0.575	V	X→Γ	1.105	0.139	0.0	False
					V	Y→S	0.842	0.097	0.285	False
					V	Γ→S	0.735	0.095	0.123	False
ISbSe	343d2125478e	P3m1 (156)	0.13	1.078	C	Γ→M	1.17	0.101	0.195	False
					C	Γ→K	0.954	0.122	0.195	False
Bi2P2Te6	cf7927ab6730	P1 (1)	0.14	0.507	C	Γ→Y	1.814	0.139	0.001	False
					C	Y→Γ	1.725	0.091	0.066	False
					C	X→Γ	1.692	0.091	0.065	False
					C	Γ→X	1.809	0.133	0.0	False
HgTe	1a3bdd1b142a	P3m1 (156)	0.165	0.132	V	Γ→M	0.501	0.107	0.01	False
					V	Γ→K	0.618	0.104	0.009	False
BiBrTe	304bc6a92d82	P3m1 (156)	0.0	0.878	V	M→K	1.13	0.112	0.502	True
					C	M→K	1.08	0.117	1.162	True
MoW3S8	2f6f133abcc8	P1 (1)	0.0	1.552	V	X→Γ	2.241	0.354	0.0	False
					C	S→Y	1.202	0.083	0.093	True
BiClSe	7fe9c5cb910c	P3m1 (156)	0.119	1.601	V	M→K	0.679	0.11	0.399	False
					C	M→Γ	0.746	0.33	0.27	False
WMo3Te8	323fb700d903	P1 (1)	0.005	0.923	V	X→Γ	1.501	0.234	0.0	False
					V	Γ→S	1.292	0.21	0.192	False
AsIS	b13beafa16aa	P3m1 (156)	0.064	1.395	V	M→K	2.033	0.22	0.442	False
					C	Γ→M	1.305	0.151	0.0	False
					C	Γ→K	1.353	0.147	0.0	True
AsITe	114b3382699c	P3m1 (156)	0.162	0.416	C	Γ→M	0.502	0.145	0.259	False
					C	Γ→K	0.579	0.166	0.221	False
WCr3Se8	c798e725e2fb	P1 (1)	0.009	0.698	V	X→Γ	1.16	0.14	0.0	False
BiIS	acdcd16c0d76	P3m1 (156)	0.014	1.139	V	M→K	1.707	0.166	0.244	True
					C	Γ→M	1.858	0.266	0.0	False
					C	M→K	1.074	0.111	1.002	True
					C	Γ→K	1.645	0.297	0.0	False
MoW3Se8	24d6cc0a0fed	Pm (6)	0.0	1.276	V	X→Γ	2.097	0.373	0.0	False
					V	Γ→S	1.24	0.236	0.293	False
Cr2Mo2S8	72b286460831	Pma2 (28)	0.017	1.039	V	X→Γ	1.344	0.095	0.0	False
					V	Y→S	0.838	0.08	0.443	False
ISSb	4c49d27e66e5	P3m1 (156)	0.185	0.872	C	Γ→M	0.887	0.113	0.409	False
					C	Γ→K	0.907	0.11	0.409	False

Entry Info					Spin Splitting Info					
Formula	C2DB ID	SG index	ΔE_{hull}	Bandgap	Band	k-path	α_R	ΔE_{SS}	$\Delta E_{VBM/CBM}$	AC
SnTe	e688959ea45b	P3m1 (156)	0.119	1.592	V	M→K	0.806	0.231	1.011	False
Ti2Zr2Se8	846b50801a93	P1 (1)	0.142	0.616	V	S→Y	1.613	0.098	0.0	False
					V	Y→S	1.767	0.098	0.0	False
					V	Γ→S	0.552	0.094	0.061	False
GeTe	eadd37f03ca5	P3m1 (156)	0.087	1.488	V	M→K	0.952	0.219	1.322	True
MoCr3Te8	899032b4ad0c	P1 (1)	0.087	0.481	V	Γ→Y	1.409	0.104	0.0	False
					V	Γ→S	0.713	0.097	0.137	False
BiIS	40034665f9f1	P3m1 (156)	0.14	0.848	C	Γ→M	1.224	0.144	0.0	False
					C	Γ→K	1.254	0.141	0.0	False
BiISe	433f707c632c	P3m1 (156)	0.114	0.84	C	Γ→M	1.228	0.153	0.0	False
					C	Γ→K	1.255	0.152	0.0	False
BiITe	a84d988e38ac	P3m1 (156)	0.11	0.691	C	M→Γ	0.467	0.132	0.566	False
O2Pb2	20f098bd3f31	Pm (6)	0.287	0.215	V	Γ→X	1.132	0.178	0.0	False
					V	Γ→Y	0.95	0.091	0.138	True
					V	Γ→S	0.875	0.132	0.036	False
					C	S→X	1.405	0.132	0.007	False
					C	S→Y	1.726	0.158	0.0	False
					C	Y→Γ	1.914	0.083	2.264	False
					C	S→Γ	1.723	0.151	0.001	False
PbSe	a0dbdc6630fa	P3m1 (156)	0.217	1.68	V	M→K	0.855	0.166	0.727	False
					C	M→Γ	1.603	0.31	0.298	False
Bi2P2Se6	aa9a981d89aa	P1 (1)	0.054	0.875	V	Γ→Y	4.457	0.217	0.005	False
					V	X→Γ	2.074	0.211	0.0	False
					V	Γ→X	4.384	0.211	0.0	False
					C	Γ→Y	1.971	0.113	0.002	False
					C	Y→Γ	1.66	0.157	0.015	False
					C	X→Γ	1.729	0.166	0.011	False
					C	Γ→X	2.029	0.113	0.0	False
HfTi3Se8	c55716558616	P1 (1)	0.137	0.589	V	S→Y	1.191	0.095	0.054	False
Mo2W2Te8	c04fc052f2ca	Pm (6)	0.011	0.879	V	X→Γ	1.645	0.259	0.0	False
					V	Γ→S	1.315	0.217	0.224	False
					C	Γ→S	1.35	0.086	0.217	False
BiISe	70cbc0e44d36	P3m1 (156)	0.0	0.929	V	M→K	1.267	0.087	0.357	False
					C	Γ→M	2.045	0.232	0.0	False
					C	M→K	1.142	0.115	1.099	False
					C	Γ→K	2.089	0.228	0.0	True
Pb2Te6	3995fa1bee6e	$P2_1(4)$	0.129	0.322	V	X→Γ	3.064	0.184	0.214	False
					V	Γ→S	0.511	0.089	0.195	False
					C	X→Γ	1.451	0.107	0.052	False
					C	X→S	0.796	0.225	0.0	False
					C	S→Γ	1.059	0.1	0.407	False
Cr2W2S8	5974b6403c31	Pma2 (28)	0.014	0.967	V	X→Γ	1.592	0.179	0.0	True
					V	Y→S	1.151	0.079	0.562	False
HfZr3Se8	70e7ab872359	P1 (1)	0.15	0.819	V	Γ→S	0.95	0.083	0.025	False
GeSe	211bcb7f05d6	P3m1 (156)	0.04	2.215	V	M→K	0.94	0.107	0.86	False
Hf2Zr2Se8	81af2831dbb2	P1 (1)	0.158	0.845	V	Γ→S	0.698	0.088	0.022	False
MoW3Te8	5c3fe56a1a89	Pm (6)	0.018	0.825	V	X→Γ	2.045	0.311	0.0	False
					V	Γ→S	1.298	0.239	0.254	False
Mo2W2S8	449640ec4d30	Pc (7)	0.0	1.553	V	X→Γ	1.954	0.278	0.0	True
					C	S→Y	1.167	0.086	0.115	True
CrW3S8	a9f87eba4b96	Pm (6)	0.009	1.144	V	X→Γ	1.909	0.28	0.0	False
CrMo3S8	644f7c1c85c7	Pm (6)	0.011	1.206	V	X→Γ	1.46	0.117	0.0	False
AsClTe	4fd8ad708fb0	P3m1 (156)	0.018	1.496	V	M→Γ	2.895	0.136	0.038	False
					V	M→K	2.257	0.127	0.462	False
CrW3Te8	eef072f845ce	P1 (1)	0.056	0.563	V	X→Γ	1.592	0.251	0.0	False
					V	Y→S	1.042	0.108	0.472	False

Formula	C2DB ID	SG index	ΔE_{hull}	Bandgap	Band	k-path	α_R	ΔE_{SS}	$\Delta E_{VBM/CBM}$	AC
	Entry Info				Spin Splitting Info					
					V	Γ→S	0.99	0.204	0.223	False
ISSb	5b94060698bc	P3m1 (156)	0.041	1.276	V	M→K	2.844	0.216	0.306	False
					C	Γ→M	1.507	0.195	0.0	False
					C	Γ→K	1.547	0.19	0.0	False
MoCr3S8	3fb52099b370	P1 (1)	0.011	0.922	V	X→Γ	1.221	0.08	0.0	False
CrW3Se8	0b7696e1f4c9	P1 (1)	0.01	0.902	V	X→Γ	1.756	0.303	0.0	False
TiHf3Te8	1667d1443160	P1 (1)	0.132	0.098	V	S→Y	1.512	0.089	0.334	False
CrMo3Te8	159f028a85d0	P1 (1)	0.035	0.665	V	Y→S	0.896	0.094	0.328	False
Ti2Zr2Te8	18e377cce57f	P1 (1)	0.118	0.143	V	S→Y	1.855	0.213	0.166	False
PbS	5e4ff1f56b4a	P3m1 (156)	0.231	1.979	C	M→Γ	1.241	0.292	0.266	True
PbTe	3bc08d486d65	P3m1 (156)	0.198	1.151	V	M→K	1.138	0.162	1.013	True
					C	M→Γ	2.18	0.319	0.208	False
P2Sb2Se6	5d1a32a28ffa	P1 (1)	0.058	1.004	V	Y→Γ	2.483	0.142	0.008	False
					V	X→Γ	2.546	0.142	0.0	False
					C	Y→Γ	1.261	0.107	0.002	False
					C	X→Γ	1.339	0.116	0.0	False
BiClTe	badda86cab42	P3m1 (156)	0.129	0.948	C	M→Γ	1.458	0.441	0.209	False
					C	M→K	0.863	0.123	0.52	True
TiZr3Te8	4f1ab08988cc	P1 (1)	0.115	0.21	V	S→Y	1.679	0.113	0.177	False
TiHf3Se8	3e1923c616ad	P1 (1)	0.166	0.722	V	S→Y	1.256	0.087	0.037	False
					V	S→Γ	0.626	0.106	0.029	False
Cr2Mo2Se8	60065d3bbcf2	P1 (1)	0.016	0.837	V	X→Γ	1.173	0.122	0.0	False
					V	Y→S	1.124	0.095	0.401	False
CrMo3Se8	a7233837cfe9	P1 (1)	0.01	0.971	V	X→Γ	1.288	0.148	0.0	False
					V	Y→S	1.311	0.097	0.498	False
					V	Γ→S	0.779	0.115	0.185	False
ZrHf3Se8	b8fb10416122	P1 (1)	0.165	0.843	V	S→Γ	0.725	0.097	0.023	False
WCr3Te8	6523c349753c	P1 (1)	0.097	0.459	V	X→Γ	0.99	0.135	0.0	False
Hf2Ti2Se8	cce78d90e899	P1 (1)	0.156	0.656	V	S→Y	1.409	0.109	0.0	False
					V	S→Γ	0.553	0.103	0.018	False
BiClSe	a80866a2c6b4	P3m1 (156)	0.0	1.139	V	Γ→M	2.393	0.118	0.018	True
					V	M→K	1.782	0.09	0.362	False
					V	Γ→K	2.216	0.124	0.0	True
					C	M→Γ	3.032	0.092	0.0	False
WMo3Se8	05a06afa3b20	Pm (6)	0.0	1.32	V	X→Γ	1.643	0.25	0.0	False
					V	Γ→S	1.001	0.195	0.232	False
BrSSb	4da5c6be60db	P3m1 (156)	0.028	1.233	V	M→K	2.39	0.117	0.28	False
Cr2W2Se8	548aa830244c	P1 (1)	0.015	0.778	V	X→Γ	1.39	0.204	0.0	False
					V	Y→S	1.322	0.128	0.497	False
WMo3S8	9c2979187585	P1 (1)	0.0	1.582	V	X→Γ	1.816	0.214	0.0	False
TiZr3Se8	a148361e5e9a	P1 (1)	0.144	0.701	V	S→Y	1.321	0.09	0.013	False
					V	Γ→S	0.88	0.086	0.041	False
BiClS	c96ef4fc869c	P3m1 (156)	0.0	1.334	C	Γ→M	1.146	0.115	0.0	True
					C	Γ→K	1.181	0.112	0.0	False
Ga2P2Te6	4cb4ea247ef4	P1 (1)	0.173	0.314	V	Y→Γ	3.695	0.163	0.001	False
					V	X→Γ	3.828	0.161	0.0	False
MoCr3Se8	961c37d6e527	Pm (6)	0.01	0.726	V	X→Γ	0.977	0.103	0.0	False
AsClSe	1a3be826b3e0	P3m1 (156)	0.013	1.364	V	Γ→M	3.717	0.097	0.039	False
					V	Γ→K	3.481	0.101	0.0	False

Dresselhaus SS Materials

Table B2. List of Dresselhaus SS prototypes identified in the valence (V) and/or conduction (C) bands for materials with non-polar structure. Each material is presented as a combination of chemical formula and its respective ID ending from the C2DB Database [1]. *SG index* represents the space group symbol (number) of the material's structure according to the precision criteria employed in this work for symmetry identification. ΔE_{hull} is the energy above the convex hull reported by the C2DB database. *Bandgap*, *k-path*, α_D, ΔE_{SS}, $\Delta E_{VBM/CBM}$ and *AC* stand for the energy band gap, k-path between high-symmetry k-points where the SS is identified, Dresselhaus coefficient (analogous to Rashba coefficient) [eV/Å^{-1}], spin-splitting magnitude, difference in energy between the maximum value of the SS and its respective band edge (VBM or CBM) and the presence of anti-crossing bands, respectively. All energy-related values are in eV.

	Entry Info				Spin Splitting Info					
Formula	C2DB ID	SG index	ΔE_{hull}	Bandgap	Band	k-path	α_D	ΔE_{SS}	$\Delta E_{VBM/CBM}$	AC
HfO2	512afaae525a	P-6m2 (187)	0.77	1.903	C	M→K	1.614	0.229	0.04	False
HgF2	f5965c8b3d89	P-4m2 (115)	0.162	1.995	V	Γ→M	0.85	0.161	0.0	False
					V	Γ→X	0.761	0.119	0.035	False
					V	X→Γ	0.324	0.115	0.035	False
					V	X→M	0.534	0.104	0.083	False
PbCl2	f9d58a299674	P-4m2 (115)	0.142	2.165	C	Γ→M	1.036	0.181	0.0	False
					C	Γ→X	1.031	0.178	0.001	False
					C	M→X	0.559	0.282	0.911	False
HfS2	3d4bfe131291	P-4m2 (115)	0.333	2.11	C	X→Γ	2.471	0.268	0.647	False
					C	M→X	1.102	0.12	0.028	True
ZrSe2	001dfe9a7fa2	P-4m2 (115)	0.319	1.452	C	X→Γ	1.998	0.101	0.521	False
O2Rh2	740bf2751050	P-6m2 (187)	0.246	0.057	V	M→K	4.914	0.11	0.0	True
PbTe2	dbf3271b4bb1	P-4m2 (115)	0.423	0.085	V	M→Γ	2.615	0.186	0.031	False
					V	Γ→M	2.556	0.171	0.031	True
					V	Γ→X	2.21	0.177	0.028	True
					C	X→M	0.846	0.104	0.101	False
PbI2	14411dde597c	P-4m2 (115)	0.145	1.531	V	M→Γ	0.951	0.244	0.0	False
					V	X→Γ	0.503	0.092	0.338	False
					V	M→X	0.931	0.229	0.037	False
					C	Γ→M	0.971	0.129	0.0	False
					C	Γ→X	0.943	0.126	0.001	False
					C	X→M	1.534	0.284	0.804	False
ZrS2	2e44a755e594	P-4m2 (115)	0.31	1.938	C	X→Γ	2.008	0.084	0.596	False
Ir2O2	06ebe3806790	P-6m2 (187)	0.51	0.099	V	M→K	4.665	0.265	0.012	True
					C	M→K	1.059	0.102	0.0	True
HgI2	7c2657e15a6f	P-4m2 (115)	0.0	1.512	C	M→Γ	0.311	0.145	0.823	False
OsBr2	bf30e1249164	P-4m2 (115)	0.677	0.092	V	X→Γ	2.633	0.121	0.0	True
					C	X→Γ	4.625	0.286	0.085	True
SnBr2	0155c4de2320	P-4m2 (115)	0.136	1.284	V	Γ→X	1.316	0.09	0.824	False
SrBr2	a4c9c803de7d	P-4m2 (115)	0.21	4.583	V	M→Γ	0.191	0.092	0.012	False
					V	M→X	0.244	0.092	0.0	False
GeI2	694ac91aec01	P-4m2 (115)	0.153	1.059	V	M→Γ	1.341	0.309	0.0	False
					V	X→Γ	0.637	0.139	0.532	False
					V	X→M	3.425	0.283	0.08	False
					C	X→M	2.307	0.16	1.134	False
HfO2	6e4ac7453419	P-4m2 (115)	0.51	4.494	C	X→Γ	0.703	0.113	0.546	False
Ir2S2	dd6289af8e01	P-6m2 (187)	0.305	0.135	C	M→K	2.202	0.164	0.0	True
PbF2	ccc95033446d	P-4m2 (115)	0.243	2.767	C	M→Γ	0.488	0.104	0.816	False
					C	X→Γ	2.465	0.082	0.0	False
OsCl2	d37ba63794ad	P-4m2 (115)	0.658	0.308	V	X→Γ	2.455	0.178	0.0	True
					C	Γ→M	1.181	0.462	0.0	False
					C	X→Γ	3.244	0.207	0.068	True
					C	X→M	0.836	0.312	0.036	False
PbBr2	cabd4ba0f21c	P-4m2 (115)	0.136	1.883	V	Γ→M	1.684	0.088	0.0	False
					V	Γ→X	0.927	0.082	0.482	False

Formula	C2DB ID	Entry Info SG index	ΔE_{hull}	Bandgap	Band	k-path	Spin Splitting Info α_D	ΔE_{SS}	$\Delta E_{VBM/CBM}$	AC
					C	Γ→M	1.072	0.161	0.0	False
					C	Γ→X	1.03	0.161	0.001	False
					C	M→X	0.425	0.259	0.921	False
HfSe2	08401460f377	P-4m2 (115)	0.337	1.676	C	X→M	3.599	0.148	0.012	False
SnI2	7f0ca28e3229	P-4m2 (115)	0.157	1.143	V	M→Γ	0.844	0.251	0.0	False
					V	Γ→M	2.545	0.258	0.0	False
					V	Γ→X	1.421	0.138	0.498	False
					V	X→M	3.076	0.224	0.031	True
					V	M→X	0.834	0.214	0.031	False
					C	X→M	2.039	0.18	1.084	True
GeBr2	204ef2affa10	P-4m2 (115)	0.136	1.312	V	M→Γ	0.353	0.114	0.0	False
					V	X→Γ	0.499	0.096	0.705	False
					V	X→M	2.998	0.092	0.009	False
					C	X→M	2.139	0.085	1.471	False
CaBr2	49f279264c91	P-4m2 (115)	0.179	4.753	V	M→Γ	0.376	0.078	0.014	False
HfTe2	1e2c6946ca41	P-4m2 (115)	0.371	1.01	C	M→Γ	1.089	0.104	0.001	True
					C	M→X	1.458	0.159	0.0	True

Zeeman SS Materials

Table B3. List of Zeeman SS prototypes identified in the valence (V) and/or conduction (C) bands for materials with all non-centrosymmetric structures. Each material is presented as a combination of chemical formula and its respective ID ending from the C2DB Database [1]. *SG index* represents the space group symbol (number) of the material's structure according to the precision criteria employed in this work for symmetry identification. ΔE_{hull} is the energy above the convex hull reported by the C2DB database. *Bandgap*, *k-point*, ΔE_{SS} and $\Delta E_{VBM/CBM}$ stand for the energy band gap, high-symmetry k-point where the SS is identified, spin-splitting magnitude and difference in energy between the maximum value of the SS and its respective band edge (VBM or CBM). All energy-related values are in eV.

Entry Info					Spin Splitting Info			
Formula	C2DB ID	SG index	ΔE_{hull}	Bandgap	Band	k-path	ΔE_{SS}	$\Delta E_{VBM/CBM}$
HgS	5256ed7d716e	P3m1 (156)	0.146	0.056	V	K	0.073	0.423
					C	K	0.047	3.733
HgO	a8678fa85c38	P-6m2 (187)	0.211	0.298	V	K	0.116	0.621
					C	K	0.013	3.96
CSiH2	8a1587098151	P3m1 (156)	0.0	4.008	C	K	0.002	1.268
ISbSe	df0019ec24b5	P3m1 (156)	0.0	1.061	V	K	0.149	0.414
					C	K	0.043	1.74
BrSbTe	f1e78a09001d	P3m1 (156)	0.13	1.331	V	K	0.078	0.586
					C	K	0.009	0.0
BrSbTe	18e62ba75259	P3m1 (156)	0.0	1.089	V	K	0.04	0.439
					C	K	0.177	1.38
ClSbSe	f705a30af945	P3m1 (156)	0.146	1.68	V	K	0.118	0.433
					C	K	0.115	0.037
BaCl2	54ec344f88a7	P-6m2 (187)	0.241	4.736	V	K	0.003	0.09
					C	K	0.018	0.08
PbS2	372c217dd52f	P-6m2 (187)	0.191	1.708	V	K	0.031	0.419
					C	K	0.73	0.636
SSeW	001e03f2c095	P3m1 (156)	0.01	1.417	V	K	0.445	0.0
					C	K	0.03	0.0
MgCl2	e73a5c5ae5ac	P-6m2 (187)	0.19	4.759	C	K	0.018	1.548
CaCl2	3ca106221b9b	P-6m2 (187)	0.164	4.784	C	K	0.012	0.402
ClITi	ae06e7424bb1	P3m1 (156)	0.115	0.746	V	K	0.063	0.0
					C	K	0.019	0.098
SnBr2	8d365ca62c55	P-6m2 (187)	0.086	2.514	V	K	0.212	0.042
					C	K	0.087	0.019
BiBrTe	f4f45fcade85	P3m1 (156)	0.117	0.916	V	K	0.065	0.718
					C	K	0.496	0.314
CdBr2	a7bb757c6234	P-6m2 (187)	0.121	2.377	V	K	0.022	0.244
					C	K	0.155	1.122
Al2O2	bce0ccee4eca	P-6m2 (187)	0.237	1.324	V	K	0.003	0.0
					C	K	0.001	0.22
HfO2	512afaae525a	P-6m2 (187)	0.77	1.903	V	K	0.018	0.22
					C	K	0.234	0.04
MoSSe	de7ac5fc6945	P3m1 (156)	0.009	1.474	V	K	0.168	0.0
					C	K	0.013	0.0
ZrSe2	f17029facf63	P-6m2 (187)	0.144	0.734	V	K	0.011	0.659
					C	K	0.124	0.65
AsBrSe	206b9dcf2af6	P3m1 (156)	0.161	1.49	V	K	0.061	0.723
					C	K	0.037	0.0
Te2Zr2	8912432cb37b	P-6m2 (187)	0.624	0.458	V	K	0.019	0.765
					C	K	0.088	0.467
Al2Te2	e54041554385	P-6m2 (187)	0.0	1.763	V	K	0.087	1.134
					C	K	0.118	0.055
Ga2S2	ac002f4ce724	P-6m2 (187)	0.0	2.305	V	K	0.02	1.322
					C	K	0.02	0.453
STeW	75ee10091f43	P3m1 (156)	0.086	1.168	V	K	0.425	0.113

Formula	C2DB ID	Entry Info SG index	ΔE_{hull}	Bandgap	Spin Splitting Info Band	k-path	ΔE_{SS}	$\Delta E_{VBM/CBM}$
					C	K	0.03	0.0
MoSTe	2ea941c8bc3c	P3m1 (156)	0.223	0.196	V	K	0.092	0.0
					C	K	0.085	0.316
CdI2	66c5fba8ad87	P-6m2 (187)	0.156	1.527	V	K	0.07	0.559
					C	K	0.289	0.377
BrITi	233dbbf8f473	P3m1 (156)	0.057	0.68	V	K	0.07	0.0
					C	K	0.019	0.078
CrTe2	c31911a1b3f9	P-6m2 (187)	0.108	0.468	V	K	0.108	0.0
					C	K	0.02	0.0
Bi2O2	53ac438f321b	P-6m2 (187)	0.319	0.449	V	K	0.155	0.623
					C	K	1.314	0.0
TiI2	088e8488f895	P-6m2 (187)	0.052	0.602	V	K	0.08	0.0
					C	K	0.018	0.024
ISbTe	0f02957b17cf	P3m1 (156)	0.0	0.886	V	K	0.07	0.553
					C	K	0.155	1.49
AsISe	ca926a42865b	P3m1 (156)	0.174	0.519	V	K	0.132	1.19
					C	K	0.069	0.135
SeTeW	6e2a4c6f4f57	P3m1 (156)	0.042	1.058	V	K	0.46	0.0
					C	K	0.042	0.0
I2Tl2	c0f52097ab62	P1 (1)	0.076	2.657	V	H	0.003	0.002
					V	H1	0.003	0.002
					C	H	0.003	0.094
					C	H1	0.003	0.094
SeSn	d59c96fdfda1	P3m1 (156)	0.098	2.156	V	K	0.115	0.55
					C	K	0.079	0.143
GeO2	77905aa4e75f	P-6m2 (187)	0.639	1.392	V	K	0.002	0.0
					C	K	0.019	3.356
BrClTi	d3f135b9cf41	P3m1 (156)	0.015	0.826	V	K	0.045	0.0
					C	K	0.011	0.216
In2Te2	fcd97ff5abcd	P-6m2 (187)	0.0	1.249	V	K	0.005	1.203
					C	K	0.143	0.793
HfI2	05a69240794c	P-6m2 (187)	0.114	0.616	V	K	0.22	0.0
					C	K	0.105	0.671
CrS2	c5ee5e35d2b4	P-6m2 (187)	0.0	0.899	V	K	0.068	0.0
					C	K	0.004	0.0
BiBrS	49b7be14f786	P3m1 (156)	0.0	1.227	V	K	0.099	0.236
					C	K	0.078	1.825
CrSeTe	5d9d3ded04de	P3m1 (156)	0.111	0.59	V	K	0.1	0.0
					C	K	0.019	0.0
AsClTe	fba4cc0df459	P3m1 (156)	0.194	1.316	V	K	0.065	0.71
					C	K	0.051	0.0
MoSeTe	42eb12e7b656	P3m1 (156)	0.025	1.159	V	K	0.2	0.0
					C	K	0.03	0.0
ClSbTe	04fdd7d1ec5c	P3m1 (156)	0.153	1.439	V	K	0.105	0.628
					C	K	0.053	0.0
SSn	f98da23471a1	P3m1 (156)	0.118	2.3	V	K	0.024	0.36
					C	K	0.141	0.115
C2O2Zr3	23672dbca7d0	P-6m2 (187)	0.211	0.381	V	K	0.009	1.323
					C	K	0.064	1.687
InN	8cf70870bc5b	P-6m2 (187)	0.482	0.606	V	K	0.016	0.0
					C	K	0.008	3.813
In2S2	172ef584c4a6	P-6m2 (187)	0.0	1.684	V	K	0.02	0.885
					C	K	0.075	1.023
BrSbSe	c2a344b393f0	P3m1 (156)	0.124	1.467	V	K	0.155	0.493
					C	K	0.071	0.078
Ag2F2	44f6ed525a5a	P1 (1)	0.048	0.52	V	H	0.047	0.236

Formula	C2DB ID	SG index	ΔE_{hull}	Bandgap	Band	k-path	ΔE_{SS}	$\Delta E_{VBM/CBM}$
	Entry Info				Spin Splitting Info			
					V	H1	0.047	0.236
					C	H	0.011	3.755
					C	H1	0.011	3.755
S2V2	605c732d5111	P-6m2 (187)	0.534	0.209	V	K	0.002	0.641
					C	K	0.047	0.052
BiBrSe	de5756e4fbfa	P3m1 (156)	0.0	1.03	V	K	0.012	0.39
					C	K	0.225	1.749
Cl2Cu2	c1a86f114149	P1 (1)	0.018	1.218	C	H	0.002	3.154
					C	H1	0.002	3.154
Bi2P2S6	287dcf4f1a19	P1 (1)	0.053	0.953	V	H	0.041	0.257
					V	H1	0.041	0.257
					C	H	0.123	0.188
					C	H1	0.123	0.188
BiClS	99fd027b1d0b	P3m1 (156)	0.12	1.841	V	K	0.062	0.298
					C	K	0.661	0.276
AsIn	c77a730c90f8	P3m1 (156)	0.4	0.681	V	K	0.031	0.108
					C	K	0.046	0.997
In2P2S6	793870f62166	P1 (1)	0.053	0.852	V	H	0.007	0.429
					V	H1	0.007	0.429
					C	H	0.003	0.372
					C	H1	0.003	0.372
ISbTe	052a3116531d	P3m1 (156)	0.123	1.031	V	K	0.051	0.682
					C	K	0.033	0.0
Se2V2	9cf30bd127fe	P-6m2 (187)	0.42	0.248	V	K	0.01	0.5
					C	K	0.045	0.07
AsGa	728f322893fe	P3m1 (156)	0.413	1.069	V	K	0.014	0.0
					C	K	0.035	0.691
AsBrS	1dcd471c2288	P3m1 (156)	0.034	1.38	V	K	0.127	0.51
					C	K	0.114	1.84
STeW	916afba26723	P3m1 (156)	0.266	0.191	V	K	0.029	0.0
					C	K	0.234	0.306
BiClTe	968a6902b7f5	P3m1 (156)	0.0	0.938	V	K	0.179	0.599
					C	K	0.722	1.354
AsBrTe	671e6de2497a	P3m1 (156)	0.163	1.098	V	K	0.133	0.673
					C	K	0.093	0.0
PbCl2	b0b142073783	P-6m2 (187)	0.105	3.136	V	K	0.067	0.0
					C	K	0.752	0.0
AsISe	5d829e480507	P3m1 (156)	0.0	1.164	V	K	0.138	0.614
					C	K	0.07	1.81
WS2	64090c9845f8	P-6m2 (187)	0.0	1.551	V	K	0.43	0.0
					C	K	0.03	0.0
O2Sc2	b757b8efeeab	P-6m2 (187)	0.249	0.694	V	K	0.01	0.173
					C	K	0.009	0.269
PbI2	9e6494406d07	P-6m2 (187)	0.078	2.029	V	K	0.002	0.218
					C	K	0.479	0.118
SnO2	d5f47e5d4cf7	P-6m2 (187)	0.645	0.623	V	K	0.004	0.0
					C	K	0.018	4.057
TiS2	65d41aaec667	P-6m2 (187)	0.145	0.721	V	K	0.005	0.515
					C	K	0.04	0.576
S2Tl2	751e767bff79	P-6m2 (187)	0.119	0.666	V	K	0.012	1.013
					C	K	0.04	1.302
O2Rh2	740bf2751050	P-6m2 (187)	0.246	0.057	V	K	0.057	0.229
					C	K	0.014	1.062
BrIZr	28c61999c692	P3m1 (156)	0.038	0.782	V	K	0.1	0.0
					C	K	0.022	0.724
ClSbSe	0c0fbdaf8f4a	P3m1 (156)	0.014	1.177	V	K	0.065	0.311

Formula	C2DB ID	SG index	ΔE_{hull}	Bandgap	Band	k-path	ΔE_{SS}	$\Delta E_{VBM/CBM}$
	Entry Info				Spin Splitting Info			
					C	K	0.261	1.795
HgI2	0ff7ee261fec	P-6m2 (187)	0.183	0.666	V	K	0.159	0.473
					C	K	0.333	0.31
ClSbTe	da5fd2bb47af	P3m1 (156)	0.008	1.291	V	K	0.148	0.324
					C	K	0.208	1.333
AsB	b6e76caa350b	P-6m2 (187)	0.467	0.752	V	K	0.002	0.0
					C	K	0.003	0.0
ZrI2	9c024b5a2e89	P-6m2 (187)	0.027	0.698	V	K	0.122	0.0
					C	K	0.026	0.586
P2Sn2Se6	a056ab5346bf	P1 (1)	0.015	0.722	V	H	0.002	0.779
					V	H1	0.002	0.779
STeZr	3f3c7bc0ce7d	P3m1 (156)	0.122	0.218	V	K	0.001	1.067
					C	K	0.133	0.386
Se2Zr2	f89b20d72c95	P-6m2 (187)	0.436	0.06	V	K	0.046	1.201
					C	K	0.039	0.51
In2Se2	eb204c739879	P-6m2 (187)	0.0	1.399	V	K	0.092	1.06
					C	K	0.021	1.148
Se2Zn2	90835c470691	Cm (8)	0.245	1.61	V	H	0.003	0.089
					V	H1	0.003	0.089
BrClZr	8cb69386d06b	P3m1 (156)	0.01	0.912	V	K	0.059	0.0
					C	K	0.008	0.987
S2Sc2	e9d256b367c7	P-6m2 (187)	0.627	0.384	V	K	0.004	0.141
					C	K	0.008	0.326
HfSSe	9afb20358166	P3m1 (156)	0.193	0.91	V	K	0.035	0.541
					C	K	0.292	0.712
P2Ru2S6	9caed1a0620c	P1 (1)	0.179	0.322	V	H	0.047	0.129
					V	H1	0.047	0.129
BiITe	2d41b3dd1772	P3m1 (156)	0.0	0.701	V	K	0.01	0.567
					C	K	0.307	1.569
Rh2Cl6	06f695e97385	P321 (150)	0.464	0.208	C	K	0.002	0.0
BaBr2	1a59eff92917	P-6m2 (187)	0.167	4.149	V	K	0.02	0.11
					C	K	0.042	0.148
Ir2O2	06ebe3806790	P-6m2 (187)	0.51	0.099	V	K	0.302	0.36
					C	K	0.207	0.639
BiBrSe	11db0908d9ef	P3m1 (156)	0.111	1.385	V	K	0.057	0.403
					C	K	0.557	0.396
Te2V2	5da53e6996e3	P-6m2 (187)	0.49	0.22	V	K	0.013	0.434
					C	K	0.068	0.038
P2Sb2Te6	82b85dfd7723	P1 (1)	0.14	0.633	V	H	0.003	0.673
					V	H1	0.003	0.673
					C	H	0.001	0.073
					C	H1	0.001	0.073
PbBr2	cbdc15b42a05	P-6m2 (187)	0.082	2.662	V	K	0.136	0.022
					C	K	0.631	0.119
Al2P2S6	669d6f1af4d4	P1 (1)	0.083	1.301	C	H	0.002	0.021
					C	H1	0.002	0.021
ISbSe	343d2125478e	P3m1 (156)	0.13	1.078	V	K	0.034	0.711
					C	K	0.028	0.171
Bi2P2Te6	cf7927ab6730	P1 (1)	0.14	0.507	V	H	0.001	0.553
					V	H1	0.001	0.553
					C	H	0.034	0.212
					C	H1	0.034	0.212
MoTe2	38a53176109a	P-6m2 (187)	0.0	0.956	V	K	0.215	0.0
					C	K	0.034	0.0
HgTe	1a3bdd1b142a	P3m1 (156)	0.165	0.132	V	K	0.095	0.446
					C	K	0.236	2.168

Entry Info					Spin Splitting Info			
Formula	C2DB ID	SG index	ΔE_{hull}	Bandgap	Band	k-path	ΔE_{SS}	$\Delta E_{VBM/CBM}$
CdCl2	46c028e03e8b	P-6m2 (187)	0.13	3.111	V	K	0.014	0.0
					C	K	0.039	1.631
BiBrTe	304bc6a92d82	P3m1 (156)	0.0	0.878	V	K	0.074	0.524
					C	K	0.597	1.437
SSeTi	358305cad463	P3m1 (156)	0.128	0.501	V	K	0.003	0.687
					C	K	0.055	0.515
ZrO2	24a8929c68ce	P-6m2 (187)	0.766	1.683	V	K	0.006	0.258
					C	K	0.065	0.026
AsIS	e23390b66883	P3m1 (156)	0.256	0.295	V	K	0.09	1.371
					C	K	0.009	0.393
MoO2	152bd69757aa	P-6m2 (187)	0.028	0.918	V	K	0.135	1.541
					C	K	0.004	0.0
BiClSe	7fe9c5cb910c	P3m1 (156)	0.119	1.601	V	K	0.114	0.411
					C	K	0.609	0.318
SrI2	6cfaae647808	P-6m2 (187)	0.096	3.448	V	K	0.022	0.182
					C	K	0.079	0.498
ZnBr2	553cb6a56984	P-6m2 (187)	0.249	2.413	V	K	0.016	0.402
					C	K	0.156	0.7
AsIS	b13beafa16aa	P3m1 (156)	0.064	1.395	V	K	0.2	0.529
					C	K	0.107	1.721
AsITe	114b3382699c	P3m1 (156)	0.162	0.416	V	K	0.189	1.022
					C	K	0.124	0.0
AsBiCr	b299416bff28	P3m1 (156)	0.461	0.037	V	K	0.041	1.339
					C	K	0.192	0.238
Ga2Se2	394e5709a3ac	P-6m2 (187)	0.0	1.736	V	K	0.011	1.375
					C	K	0.036	0.847
Sc2Te2	c3cac8e74dc1	P-6m2 (187)	0.614	0.287	V	K	0.002	0.051
					C	K	0.006	0.112
BaI2	c4707a226b8f	P-6m2 (187)	0.105	3.362	V	K	0.043	0.155
					C	K	0.075	0.267
BiIS	acdcd16c0d76	P3m1 (156)	0.014	1.139	V	K	0.164	0.26
					C	K	0.236	1.612
HgCl2	6cbe2e585099	P-6m2 (187)	0.131	2.023	V	K	0.073	0.0
					C	K	0.048	1.125
GaN	c973e283b023	P-6m2 (187)	0.416	1.818	V	K	0.006	0.0
					C	K	0.001	3.052
Te2Tl2	73117163f0e2	P-6m2 (187)	0.137	0.367	V	K	0.149	1.151
					C	K	0.368	0.566
N2O2Hf3	bb4e40ae9164	P-6m2 (187)	0.088	0.323	V	K	0.1	0.0
					C	K	0.115	1.31
ISSb	4c49d27e66e5	P3m1 (156)	0.185	0.872	V	K	0.057	0.853
					C	K	0.085	0.327
Br2Tl2	948c61cd5626	P1 (1)	0.063	3.311	V	H	0.002	0.034
					V	H1	0.002	0.034
					C	H	0.002	0.006
					C	H1	0.002	0.006
Rh2Br6	c284d6de2b3e	P3 (143)	0.408	0.26	C	K	0.004	0.002
SnS2	8f2fa65321f0	P-6m2 (187)	0.286	0.754	V	K	0.005	0.186
					C	K	0.042	0.818
ClSSb	9188c300265c	P3m1 (156)	0.048	1.332	V	K	0.013	0.236
					C	K	0.313	1.878
SnTe	e688959ea45b	P3m1 (156)	0.119	1.592	V	K	0.228	1.08
					C	K	0.003	0.18
HfCl2	864f8b497185	P-6m2 (187)	0.007	0.891	V	K	0.099	0.0
					C	K	0.236	1.274
Cl2Pt2	93dfef2d1004	P1 (1)	0.0	1.329	V	H	0.002	0.393

Entry Info					Spin Splitting Info			
Formula	C2DB ID	SG index	ΔE_{hull}	Bandgap	Band	k-path	ΔE_{SS}	$\Delta E_{VBM/CBM}$
					V	H1	0.002	0.393
MoS2	b3b4685fb6e1	P-6m2 (187)	0.0	1.603	V	K	0.148	0.0
					C	K	0.003	0.0
SrCl2	77398c835c11	P-6m2 (187)	0.194	4.958	V	K	0.001	0.051
					C	K	0.009	0.312
ClIZr	73202b4b7837	P3m1 (156)	0.078	0.883	V	K	0.087	0.0
					C	K	0.021	0.716
GeTe	eadd37f03ca5	P3m1 (156)	0.087	1.488	V	K	0.188	1.475
					C	K	0.079	0.283
CaBr2	fbb623b6f288	P-6m2 (187)	0.129	4.141	V	K	0.003	0.05
					C	K	0.04	0.485
BrHfI	836a1091409d	P3m1 (156)	0.087	0.695	V	K	0.182	0.0
					C	K	0.193	0.856
CrSSe	09e1e5ef94cb	P3m1 (156)	0.01	0.802	V	K	0.082	0.0
					C	K	0.01	0.0
ZrTe2	f7ad606317e6	P-6m2 (187)	0.11	0.275	V	K	0.01	0.802
					C	K	0.163	0.741
Ir2Cl6	be7870547213	P321 (150)	0.555	0.263	C	K	0.003	0.0
SrBr2	2876a0cb2478	P-6m2 (187)	0.14	4.324	V	K	0.008	0.067
					C	K	0.038	0.415
CrSe2	9a6ff6a3c41a	P-6m2 (187)	0.0	0.703	V	K	0.09	0.0
					C	K	0.015	0.0
SnCl2	514a8a12dca9	P-6m2 (187)	0.117	2.76	V	K	0.065	0.0
					C	K	0.187	0.039
OSn	026ebfd86b48	P3m1 (156)	0.329	1.682	V	K	0.009	0.0
					C	K	0.137	0.825
HfS2	2c5e65012601	P-6m2 (187)	0.217	1.082	V	K	0.033	0.471
					C	K	0.272	0.712
AsClS	0fd6ab210774	P3m1 (156)	0.224	1.732	V	K	0.055	0.648
					C	K	0.063	0.088
Ir2S2	dd6289af8e01	P-6m2 (187)	0.305	0.135	V	K	0.241	0.183
					C	K	0.221	0.859
ZrCl2	dc09b7c396eb	P-6m2 (187)	0.0	0.988	V	K	0.041	0.0
					C	K	0.001	1.06
BiIS	40034665f9f1	P3m1 (156)	0.14	0.848	V	K	0.097	0.799
					C	K	0.553	0.435
GaP	d467820f3f04	P3m1 (156)	0.447	1.555	V	K	0.007	0.0
					C	K	0.005	0.563
Al2S2	f9df9f4a5c34	P-6m2 (187)	0.005	2.099	V	K	0.012	0.654
					C	K	0.01	0.069
HfSSe	63618e5bf062	P3m1 (156)	0.0	0.705	V	K	0.024	2.114
					C	K	0.002	1.466
BiISe	433f707c632c	P3m1 (156)	0.114	0.84	V	K	0.118	0.642
					C	K	0.495	0.459
AlAs	814ae25a188e	P-6m2 (187)	0.522	1.241	V	K	0.002	0.0
					C	K	0.002	1.092
ZrBr2	7897c7cc2491	P-6m2 (187)	0.0	0.827	V	K	0.076	0.0
					C	K	0.012	0.948
AsBrSe	989f469f06bd	P3m1 (156)	0.0	1.212	V	K	0.061	0.576
					C	K	0.069	1.752
ZrS2	1a039e022308	P-6m2 (187)	0.19	0.97	V	K	0.01	0.572
					C	K	0.087	0.567
HgSe	619ed885f677	P3m1 (156)	0.157	0.069	V	K	0.061	0.375
					C	K	0.136	2.954
BiITe	a84d988e38ac	P3m1 (156)	0.11	0.691	V	K	0.163	0.588
					C	K	0.43	0.387

Entry Info					Spin Splitting Info			
Formula	C2DB ID	SG index	ΔE_{hull}	Bandgap	Band	k-path	ΔE_{SS}	$\Delta E_{VBM/CBM}$
AsBrTe	64921449e408	P3m1 (156)	0.0	1.253	V	K	0.005	0.611
					C	K	0.028	1.261
SSeZr	1a9901838600	P3m1 (156)	0.0	0.616	V	K	0.039	1.958
					C	K	0.007	1.241
P2Ta2Te6	601435d29c97	P1 (1)	0.222	0.206	C	H	0.001	0.107
					C	H1	0.001	0.107
GeCl2	a7216f084785	P-6m2 (187)	0.136	2.955	V	K	0.067	0.112
					C	K	0.057	0.0
TiBr2	57116f9a9a4e	P-6m2 (187)	0.0	0.756	V	K	0.056	0.0
					C	K	0.015	0.172
WO2	94cfbb3f9284	P-6m2 (187)	0.0	1.312	V	K	0.406	1.385
					C	K	0.02	0.0
Hg2P2S6	b81eb586acfd	P1 (1)	0.0	0.981	C	H	0.001	0.731
					C	H1	0.001	0.731
GeBr2	36a198743d35	P-6m2 (187)	0.112	2.543	V	K	0.175	0.251
					C	K	0.042	0.0
SSeZr	2be14f373da0	P3m1 (156)	0.163	0.831	V	K	0.008	0.623
					C	K	0.107	0.569
MoSe2	f61b14d398c7	P-6m2 (187)	0.0	1.342	V	K	0.185	0.0
					C	K	0.021	0.0
BrSbSe	89b15ddef41d	P3m1 (156)	0.0	1.072	V	K	0.044	0.383
					C	K	0.231	1.758
WSe2	1cfbe6183886	P-6m2 (187)	0.0	1.255	V	K	0.466	0.0
					C	K	0.037	0.0
PbSe	a0dbdc6630fa	P3m1 (156)	0.217	1.68	V	K	0.158	0.845
					C	K	0.431	0.647
CaI2	066f40f26c53	P-6m2 (187)	0.108	2.995	V	K	0.011	0.412
					C	K	0.079	0.582
Bi2P2Se6	aa9a981d89aa	P1 (1)	0.054	0.875	C	H	0.149	0.09
					C	H1	0.149	0.09
HfSeTe	305c779b8752	P3m1 (156)	0.149	0.16	V	K	0.035	1.04
					C	K	0.321	0.727
HfTe2	59c0e014651d	P-6m2 (187)	0.133	0.147	V	K	0.04	0.902
					C	K	0.343	0.848
AlSb	1734deee2ac1	P3m1 (156)	0.475	1.447	V	K	0.02	0.0
					C	K	0.046	0.017
BiISe	70cbc0e44d36	P3m1 (156)	0.0	0.929	V	K	0.087	0.383
					C	K	0.08	1.731
GeO	a42f736f1682	P3m1 (156)	0.311	2.093	V	K	0.008	0.0
					C	K	0.059	0.757
BrSSb	4ae37f15e1fe	P3m1 (156)	0.157	1.437	V	K	0.139	0.444
					C	K	0.129	0.21
TiCl2	95688ba68ca1	P-6m2 (187)	0.001	0.901	V	K	0.032	0.0
					C	K	0.004	0.281
Rh2Se2	1a46a7cf8fab	P-6m2 (187)	0.164	0.063	V	K	0.136	0.638
					C	K	0.024	0.356
AsClSe	df329350eef2	P3m1 (156)	0.179	1.71	V	K	0.05	0.702
					C	K	0.004	0.0
GeSe	211bcb7f05d6	P3m1 (156)	0.04	2.215	V	K	0.109	0.914
					C	K	0.009	0.272
ClHfI	d3756ea15451	P3m1 (156)	0.14	0.806	V	K	0.158	0.0
					C	K	0.204	0.889
TiSe2	509ef368050d	P-6m2 (187)	0.117	0.515	V	K	0.004	0.602
					C	K	0.064	0.581
Sc2Se2	9fb15588e4d4	P-6m2 (187)	0.548	0.373	V	K	0.004	0.092
					C	K	0.007	0.185

Entry Info					Spin Splitting Info			
Formula	C2DB ID	SG index	ΔE_{hull}	Bandgap	Band	k-path	ΔE_{SS}	$\Delta E_{VBM/CBM}$
In2O2	d14171d2ba1a	P-6m2 (187)	0.208	0.371	V	K	0.008	0.0
					C	K	0.073	2.911
Ag2Cl2	dd5f0964d63d	P1 (1)	0.003	1.597	C	H	0.002	3.303
					C	H1	0.002	3.303
C2O2Hf3	082ae1b027e9	P-6m2 (187)	0.216	0.419	V	K	0.007	1.227
					C	K	0.214	1.853
HfBr2	84e9162c0c53	P-6m2 (187)	0.004	0.722	V	K	0.149	0.0
					C	K	0.191	1.089
BrClHf	72257f9ad66d	P3m1 (156)	0.016	0.819	V	K	0.126	0.0
					C	K	0.222	1.164
AsClS	afd0d75a82a2	P3m1 (156)	0.056	1.532	V	K	0.018	0.466
					C	K	0.126	1.781
TiO2	1cfb690281c9	P-6m2 (187)	0.587	1.136	V	K	0.003	0.416
					C	K	0.035	0.141
OPb	2a393480e273	P3m1 (156)	0.315	1.806	V	K	0.018	0.106
					C	K	0.442	1.675
InSb	466fcf7fad66	P3m1 (156)	0.379	0.477	V	K	0.054	0.233
					C	K	0.098	0.598
AsClTe	4fd8ad708fb0	P3m1 (156)	0.018	1.496	V	K	0.112	0.475
					C	K	0.038	1.159
Se2Tl2	625697b299d1	P-6m2 (187)	0.076	0.488	V	K	0.051	1.134
					C	K	0.178	1.062
CrSTe	8a0864d30ce1	P3m1 (156)	0.161	0.288	V	K	0.095	0.4
					C	K	0.018	0.0
ISSb	5b94060698bc	P3m1 (156)	0.041	1.276	V	K	0.216	0.314
					C	K	0.193	1.644
Ir2Se2	53337987551a	P-6m2 (187)	0.426	0.287	V	K	0.367	0.202
					C	K	0.248	0.499
PbSe2	0bc5d11454a7	P-6m2 (187)	0.18	1.324	V	K	0.135	0.386
					C	K	0.192	0.721
BiBrS	3b305c3e2c18	P3m1 (156)	0.116	1.594	V	K	0.086	0.335
					C	K	0.61	0.357
PdSe2	0ae696751911	P-6m2 (187)	0.268	0.231	V	K	0.345	1.632
					C	K	0.026	0.106
CSiF2	ee1174d1d821	P3m1 (156)	0.6	1.91	V	K	0.01	2.415
					C	K	0.003	4.272
Te2Ti2	b43c14735d8e	P-6m2 (187)	0.61	0.232	V	K	0.012	0.704
					C	K	0.059	0.196
N2O2Zr3	c317fbd68215	P-6m2 (187)	0.094	0.404	V	K	0.031	0.013
					C	K	0.052	1.018
ZnI2	701e1fc14b22	P-6m2 (187)	0.302	0.931	V	K	0.072	0.718
					C	K	0.283	0.477
PbS	5e4ff1f56b4a	P3m1 (156)	0.231	1.979	V	K	0.019	0.699
					C	K	0.489	0.588
InP	c5672c6c1c78	P3m1 (156)	0.432	1.072	V	K	0.02	0.0
					C	K	0.011	1.071
SeTeZr	dd69b684c867	P3m1 (156)	0.115	0.275	V	K	0.005	0.945
					C	K	0.146	0.595
PbTe	3bc08d486d65	P3m1 (156)	0.198	1.151	V	K	0.345	1.28
					C	K	0.357	0.573
SnI2	d9c422656482	P-6m2 (187)	0.085	1.965	V	K	0.182	0.251
					C	K	0.025	0.0
P2Sb2Se6	5d1a32a28ffa	P1 (1)	0.058	1.004	V	H	0.002	0.671
					V	H1	0.002	0.671
					C	H	0.057	0.121
					C	H1	0.057	0.121

Formula	C2DB ID	Entry Info SG index	ΔE_{hull}	Bandgap	Spin Splitting Info Band	k-path	ΔE_{SS}	$\Delta E_{VBM/CBM}$
AsBrS	d9f4d4011670	P3m1 (156)	0.201	1.425	V	K	0.011	0.769
					C	K	0.022	0.208
BiClTe	badda86cab42	P3m1 (156)	0.129	0.948	V	K	0.043	0.929
					C	K	0.553	0.239
MoSTe	e4bb8738150a	P3m1 (156)	0.065	1.027	V	K	0.186	0.27
					C	K	0.026	0.0
CrO2	2433700165bb	P-6m2 (187)	0.168	0.422	V	K	0.064	1.123
					C	K	0.002	0.0
MgI2	67bb6819958f	P-6m2 (187)	0.16	2.601	V	K	0.024	0.683
					C	K	0.208	0.497
HgBr2	9965e7e32aa2	P-6m2 (187)	0.12	1.521	V	K	0.076	0.18
					C	K	0.189	0.69
Hg2I2	f7e70d2b90ad	P1 (1)	0.0	1.265	V	H	0.001	0.65
					V	H1	0.001	0.65
HfSe2	d2d9fee03594	P-6m2 (187)	0.174	0.827	V	K	0.037	0.564
					C	K	0.311	0.778
Ga2O2	16c96094d1a0	P-6m2 (187)	0.06	1.48	V	K	0.007	0.063
					C	K	0.025	2.204
WCr3Te8	6523c349753c	P1 (1)	0.097	0.459	C	Y	0.001	0.222
ClSSb	0495f35048b5	P3m1 (156)	0.179	1.675	V	K	0.058	0.354
					C	K	0.174	0.147
BiClSe	a80866a2c6b4	P3m1 (156)	0.0	1.139	V	K	0.089	0.362
					C	K	0.355	1.732
O2W2	42fa50003592	P-6m2 (187)	0.503	0.04	V	K	0.237	0.428
					C	K	0.063	0.807
ZnCl2	62c6ee7a0a25	P-6m2 (187)	0.236	3.437	V	K	0.008	0.126
					C	K	0.039	1.109
BrSSb	4da5c6be60db	P3m1 (156)	0.028	1.233	V	K	0.117	0.28
					C	K	0.244	1.825
BSb	71730c0eaab1	P-6m2 (187)	0.806	0.301	V	K	0.013	0.0
					C	K	0.01	0.0
WTe2	3c87365bc48c	P-6m2 (187)	0.026	0.754	V	K	0.485	0.0
					C	K	0.052	0.0
Al2Se2	129a514b51ad	P-6m2 (187)	0.0	1.997	V	K	0.051	0.957
					C	K	0.056	0.063
GeS	227b12019ade	P3m1 (156)	0.053	2.467	V	K	0.024	0.692
					C	K	0.051	0.172
BiClS	c96ef4fc869c	P3m1 (156)	0.0	1.334	V	K	0.006	0.254
					C	K	0.206	1.839
Ga2P2Te6	4cb4ea247ef4	P1 (1)	0.173	0.314	V	H	0.143	0.629
					V	H1	0.143	0.629
					C	H	0.103	0.0
					C	H1	0.103	0.0
MgBr2	bee1987fb4e6	P-6m2 (187)	0.169	3.569	V	K	0.003	0.37
					C	K	0.08	1.554
AsITe	b6d803aafe3a	P3m1 (156)	0.0	1.009	V	K	0.074	0.715
					C	K	0.022	1.44
AsClSe	1a3be826b3e0	P3m1 (156)	0.013	1.364	V	K	0.051	0.508
					C	K	0.08	1.706
Ga2Te2	55c23ca88a05	P-6m2 (187)	0.002	1.289	V	K	0.02	1.202

High-Order SS Materials

Table B4. List of High-Order SS prototypes identified in the valence (V) and/or conduction (C) bands for materials with all non-centrosymmetric structures. Each material is presented as a combination of chemical formula and its respective ID ending from the C2DB Database [1]. *SG index* represents the space group symbol (number) of the material's structure according to the precision criteria employed in this work for symmetry identification. ΔE_{hull} is the energy above convex hull reported by the C2DB database. *Bandgap*, *k-path*, ΔE_{SS}, $\Delta E_{VBM/CBM}$ and *AC* stand for the energy band gap, k-path between high-symmetry k-points where the SS is identified, spin-splitting magnitude, difference in energy between the maximum value of the SS and its respective band edge (VBM or CBM) and the presence of anti-crossing bands, respectively. All energy-related values are in eV.

Entry Info					Spin Splitting Info				
Formula	C2DB ID	SG index	ΔE_{hull}	Bandgap	Band	k-point	ΔE_{SS}	$\Delta E_{VBM/CBM}$	AC
HgS	5256ed7d716e	P3m1 (156)	0.146	0.056	V	Γ→M	0.017	0.006	False
					V	Γ→K	0.035	0.0	False
ISbSe	df0019ec24b5	P3m1 (156)	0.0	1.061	V	Γ→M	0.002	0.493	True
					V	Γ→K	0.003	0.492	True
BrSbTe	18e62ba75259	P3m1 (156)	0.0	1.089	C	Γ→K	0.167	1.381	False
ClSbSe	f705a30af945	P3m1 (156)	0.146	1.68	V	Γ→M	0.073	0.104	False
					V	Γ→K	0.107	0.0	False
SSeW	001e03f2c095	P3m1 (156)	0.01	1.417	V	M→Γ	0.019	1.265	False
TiSe2	0684166af1fd	P-4m2 (115)	0.261	0.864	V	Γ→X	0.01	0.909	False
					C	M→Γ	0.015	0.0	False
					C	M→X	0.02	0.057	False
SnBr2	8d365ca62c55	P-6m2 (187)	0.086	2.514	C	M→K	0.069	0.08	False
BiBrTe	f4f45fcade85	P3m1 (156)	0.117	0.916	V	Γ→M	0.013	0.782	False
TiO2	badf6957f0bb	P-4m2 (115)	0.213	3.422	V	M→Γ	0.014	0.098	False
					V	X→M	0.015	0.023	False
					V	M→X	0.015	0.023	False
					C	X→Γ	0.014	1.037	False
GeSe2	8af45b2cf14e	P-4m2 (115)	0.051	0.556	V	Γ→X	0.029	0.349	False
					V	X→M	0.006	0.883	False
					C	Γ→M	0.175	1.404	False
					C	Γ→X	0.039	0.328	False
ZrSe2	f17029facf63	P-6m2 (187)	0.144	0.734	V	Γ→K	0.097	0.0	False
SrF2	c99805c05244	P-4m2 (115)	0.376	6.025	C	X→M	0.001	6.025	False
AsBrSe	206b9dcf2af6	P3m1 (156)	0.161	1.49	C	M→K	0.058	0.433	False
Al2Te2	e54041554385	P-6m2 (187)	0.0	1.763	C	M→K	0.097	0.388	False
Ga2S2	ac002f4ce724	P-6m2 (187)	0.0	2.305	C	M→K	0.012	0.656	False
STeW	75ee10091f43	P3m1 (156)	0.086	1.168	V	M→Γ	0.046	0.951	False
MoSTe	2ea941c8bc3c	P3m1 (156)	0.223	0.196	C	M→Γ	0.011	0.252	False
HgF2	f5965c8b3d89	P-4m2 (115)	0.162	1.995	V	M→Γ	0.161	0.0	False
					C	X→Γ	0.002	0.0	False
CdBr2	bb3c9722fb14	P-4m2 (115)	0.02	2.939	V	X→M	0.01	0.0	False
					C	X→M	0.004	0.0	False
SnO2	96a036411ab6	P-4m2 (115)	0.434	2.065	V	M→Γ	0.01	0.101	False
					V	Γ→M	0.01	0.118	False
GeO2	21281ac194c2	P-4m2 (115)	0.152	2.944	V	M→Γ	0.014	0.166	False
					C	X→M	0.003	4.194	False
Sn2Te2	03bcf7dcdaf2	$Pmn2_1$(31)	0.063	0.595	C	S→Y	0.006	0.153	False
					C	Y→S	0.006	0.153	False
					C	S→Γ	0.012	0.412	False
AsISe	ca926a42865b	P3m1 (156)	0.174	0.519	C	M→K	0.07	0.547	False
SeTeW	6e2a4c6f4f57	P3m1 (156)	0.042	1.058	V	M→Γ	0.033	1.041	False
Pb2S2	d4ed2cd9ee0c	$Pmn2_1$(31)	0.054	1.341	V	Y→Γ	0.003	0.001	False
					C	S→Y	0.014	0.211	False
					C	Y→S	0.014	0.211	False
					C	Y→Γ	0.012	0.0	False
					C	S→Γ	0.005	0.649	False

Entry Info					Spin Splitting Info				
Formula	C2DB ID	SG index	ΔE_{hull}	Bandgap	Band	k-point	ΔE_{SS}	$\Delta E_{VBM/CBM}$	AC
ZrO2	da3987f48688	P-4m2 (115)	0.464	4.378	V	X→Γ	0.004	0.683	False
I2Tl2	c0f52097ab62	P1 (1)	0.076	2.657	C	C→H1	0.003	0.094	False
					C	X→H1	0.003	0.094	False
SeSn	d59c96fdfda1	P3m1 (156)	0.098	2.156	V	M→Γ	0.053	0.025	False
					C	Γ→M	0.143	0.781	False
					C	Γ→K	0.232	0.923	False
CdF2	14736784891b	P-4m2 (115)	0.208	3.802	C	X→M	0.001	0.0	False
BrClTi	d3f135b9cf41	P3m1 (156)	0.015	0.826	C	M→Γ	0.01	0.047	False
CrS2	c5ee5e35d2b4	P-6m2 (187)	0.0	0.899	C	M→K	0.017	0.273	False
BiBrS	49b7be14f786	P3m1 (156)	0.0	1.227	V	Γ→M	0.051	0.037	False
					V	M→K	0.099	0.236	False
					V	Γ→K	0.057	0.0	False
CrSeTe	5d9d3ded04de	P3m1 (156)	0.111	0.59	C	Γ→M	0.003	0.389	False
					C	Γ→K	0.042	0.292	False
PbCl2	f9d58a299674	P-4m2 (115)	0.142	2.165	V	Γ→M	0.004	0.0	False
					V	Γ→X	0.025	0.715	False
AsClTe	fba4cc0df459	P3m1 (156)	0.194	1.316	V	M→Γ	0.019	0.856	False
					C	M→Γ	0.016	0.242	False
MoSeTe	42eb12e7b656	P3m1 (156)	0.025	1.159	V	M→Γ	0.009	0.84	False
					C	Γ→M	0.018	0.332	False
					C	Γ→K	0.028	0.122	False
BaF2	4b7403281822	P-4m2 (115)	0.375	5.659	V	X→Γ	0.002	0.017	False
ClSbTe	04fdd7d1ec5c	P3m1 (156)	0.153	1.439	C	Γ→M	0.002	0.314	False
					C	Γ→K	0.076	0.315	False
SSn	f98da23471a1	P3m1 (156)	0.118	2.3	V	M→Γ	0.01	0.028	False
					C	M→K	0.084	0.287	False
InN	8cf70870bc5b	P-6m2 (187)	0.482	0.606	V	Γ→K	0.01	1.186	False
In2S2	172ef584c4a6	P-6m2 (187)	0.0	1.684	C	M→K	0.052	1.091	False
BrSbSe	c2a344b393f0	P3m1 (156)	0.124	1.467	V	Γ→M	0.01	0.138	False
					V	Γ→K	0.123	0.0	False
					C	M→K	0.084	0.297	False
Ag2F2	44f6ed525a5a	P1 (1)	0.048	0.52	C	Γ→Y	0.011	3.873	False
					C	Y→H	0.011	3.873	False
S2V2	605c732d5111	P-6m2 (187)	0.534	0.209	C	M→K	0.029	0.0	False
					C	Γ→K	0.022	0.007	False
HfS2	3d4bfe131291	P-4m2 (115)	0.333	2.11	V	X→M	0.012	0.671	False
					C	M→Γ	0.119	0.0	False
PbSe2	45aa9714a72b	P-4m2 (115)	0.372	0.286	V	X→M	0.006	0.0	False
					C	Γ→M	0.167	0.862	False
					C	Γ→X	0.036	0.281	False
SrI2	1059dc7f5fe4	P-4m2 (115)	0.188	3.964	C	Γ→M	0.025	0.811	False
Bi2P2S6	287dcf4f1a19	P1 (1)	0.053	0.953	V	X→H1	0.052	0.376	False
CdCl2	ff50eed37ec7	P-4m2 (115)	0.043	3.632	C	Γ→X	0.001	2.312	False
AsIn	c77a730c90f8	P3m1 (156)	0.4	0.681	V	Γ→M	0.005	0.985	False
					V	Γ→K	0.064	1.058	False
					C	Γ→M	0.082	1.406	False
					C	M→Γ	0.082	1.406	False
					C	Γ→K	0.121	1.669	False
In2P2S6	793870f62166	P1 (1)	0.053	0.852	V	Γ→Y	0.005	0.0	False
					V	Γ→X	0.005	0.0	False
ZrSe2	001dfe9a7fa2	P-4m2 (115)	0.319	1.452	V	Γ→M	0.058	0.784	False
					V	Γ→X	0.032	0.812	False
					V	X→M	0.032	0.812	False
TiTe2	bbb8e581bf27	P-4m2 (115)	0.338	0.397	V	Γ→X	0.014	0.958	False
					V	X→M	0.014	0.669	False
					C	M→Γ	0.014	0.0	False

Formula	C2DB ID	SG index	ΔE_{hull}	Bandgap	Band	k-point	ΔE_{SS}	$\Delta E_{VBM/CBM}$	AC
	Entry Info				Spin Splitting Info				
					C	M→X	0.016	0.033	False
ISbTe	052a3116531d	P3m1 (156)	0.123	1.031	C	M→Γ	0.026	0.311	False
Se2V2	9cf30bd127fe	P-6m2 (187)	0.42	0.248	C	M→K	0.04	0.0	False
AsGa	728f322893fe	P3m1 (156)	0.413	1.069	V	Γ→M	0.016	1.087	False
					V	M→Γ	0.016	1.087	False
					V	Γ→K	0.043	1.243	False
					C	Γ→M	0.08	1.418	False
					C	M→Γ	0.08	1.418	False
					C	Γ→K	0.122	1.784	False
AsBrS	1dcd471c2288	P3m1 (156)	0.034	1.38	V	Γ→M	0.054	0.053	False
					V	Γ→K	0.068	0.0	False
AsBrTe	671e6de2497a	P3m1 (156)	0.163	1.098	V	M→Γ	0.012	0.938	False
Pb2Se2	f615d3b872f4	$Pmn2_1$(31)	0.072	0.949	V	Y→Γ	0.005	0.002	False
					C	S→Y	0.012	0.223	False
					C	Y→S	0.012	0.223	False
					C	Y→Γ	0.006	0.0	False
					C	S→Γ	0.004	0.571	False
AsISe	5d829e480507	P3m1 (156)	0.0	1.164	V	Γ→K	0.06	0.214	True
ZrHf3Te8	3663f526cdf1	P1 (1)	0.127	0.165	V	S→X	0.004	0.454	False
					V	Y→S	0.004	0.421	False
					V	Γ→S	0.018	0.165	False
					C	S→X	0.002	0.254	False
BrIZr	28c61999c692	P3m1 (156)	0.038	0.782	C	M→Γ	0.006	0.088	False
					C	M→K	0.022	1.038	False
ClSbSe	0c0fbdaf8f4a	P3m1 (156)	0.014	1.177	V	M→Γ	0.093	0.035	False
					C	M→K	0.222	1.824	False
					C	Γ→K	0.227	1.799	False
ClSbTe	da5fd2bb47af	P3m1 (156)	0.008	1.291	V	Γ→M	0.127	0.034	False
					V	Γ→K	0.168	0.0	False
					C	M→K	0.19	1.442	False
					C	Γ→K	0.125	1.373	False
PbI2	14411dde597c	P-4m2 (115)	0.145	1.531	V	Γ→M	0.247	0.0	False
					V	Γ→X	0.092	0.338	False
ZrS2	2e44a755e594	P-4m2 (115)	0.31	1.938	V	Γ→M	0.022	0.637	False
					C	M→Γ	0.042	0.0	False
					C	M→X	0.035	0.086	False
ZnI2	ce0e9cd74bb3	P-4m2 (115)	0.0	2.467	V	X→M	0.022	2.467	False
PbO2	8d2de90b58b6	P-4m2 (115)	0.339	1.084	V	Γ→X	0.004	0.053	False
					C	X→Γ	0.002	0.0	False
STeZr	3f3c7bc0ce7d	P3m1 (156)	0.122	0.218	C	M→Γ	0.01	0.0	False
Se2Zr2	f89b20d72c95	P-6m2 (187)	0.436	0.06	C	Γ→K	0.037	0.0	False
Hf2Zr2S8	540829ada792	P1 (1)	0.2	1.145	V	S→Y	0.018	0.0	False
					V	Y→S	0.018	0.0	False
					C	X→S	0.012	0.132	False
HfZr3S8	78bb1ac31c01	P1 (1)	0.193	1.145	V	Γ→X	0.002	0.0	False
					V	S→Y	0.017	0.02	False
					V	Y→S	0.017	0.02	False
					V	Y→Γ	0.005	0.07	False
					C	X→S	0.016	0.111	False
Cr2W2Te8	62bb754c4cb2	Pm (6)	0.082	0.512	V	S→Γ	0.136	0.16	False
					C	Γ→X	0.008	0.0	False
Mo2W2Se8	a1d716aad84d	P1 (1)	0.0	1.288	V	S→Γ	0.224	0.262	False
					C	X→Γ	0.011	0.0	True
BrClZr	8cb69386d06b	P3m1 (156)	0.01	0.912	C	M→K	0.018	1.368	False
HfSSe	9afb20358166	P3m1 (156)	0.193	0.91	C	M→Γ	0.008	0.0	False
P2Ru2S6	9caed1a0620c	P1 (1)	0.179	0.322	V	Γ→Y	0.072	0.0	False

Entry Info					Spin Splitting Info				
Formula	C2DB ID	SG index	ΔE_{hull}	Bandgap	Band	k-point	ΔE_{SS}	$\Delta E_{VBM/CBM}$	AC
					V	Γ→X	0.073	0.0	False
					C	Y→H	0.004	0.0	False
					C	C→H	0.004	0.0	False
					C	C→H1	0.004	0.0	False
					C	X→H1	0.004	0.0	False
BiITe	2d41b3dd1772	P3m1 (156)	0.0	0.701	V	Γ→M	0.11	0.012	False
					V	Γ→K	0.131	0.0	False
ZrHf3S8	9cbc09153aeb	P1 (1)	0.208	1.152	V	S→Y	0.02	0.008	False
					V	Y→S	0.02	0.008	False
					V	Y→Γ	0.007	0.068	False
					V	Γ→S	0.017	0.034	False
					C	X→S	0.015	0.135	False
					C	Γ→Y	0.007	0.0	False
ZrTi3Se8	52a5e2b280d4	P1 (1)	0.131	0.571	V	S→X	0.015	0.249	False
					C	X→Γ	0.033	0.161	False
Ir2O2	06ebe3806790	P-6m2 (187)	0.51	0.099	C	Γ→K	0.11	0.373	False
Te2V2	5da53e6996e3	P-6m2 (187)	0.49	0.22	C	M→K	0.054	0.0	False
HgI2	7c2657e15a6f	P-4m2 (115)	0.0	1.512	V	X→M	0.019	0.0	False
P2Sb2Te6	82b85dfd7723	P1 (1)	0.14	0.633	V	Γ→Y	0.226	0.007	False
					V	Γ→X	0.223	0.0	False
WCr3S8	dc4259e69783	Pmm2 (25)	0.009	0.887	C	X→Γ	0.007	0.0	False
Al2P2S6	669d6f1af4d4	P1 (1)	0.083	1.301	V	Y→Γ	0.01	0.0	False
					V	X→Γ	0.01	0.0	False
					C	Γ→Y	0.002	0.663	False
					C	Γ→X	0.002	0.667	False
Cr2Mo2Te8	988b11badabb	P1 (1)	0.067	0.575	V	S→Γ	0.095	0.123	False
ISbSe	343d2125478e	P3m1 (156)	0.13	1.078	C	M→Γ	0.069	0.34	False
					C	M→K	0.055	0.394	False
Bi2P2Te6	cf7927ab6730	P1 (1)	0.14	0.507	V	Γ→Y	0.241	0.004	False
					V	Y→Γ	0.241	0.004	False
					V	X→Γ	0.239	0.0	False
					V	Γ→X	0.239	0.0	False
HgTe	1a3bdd1b142a	P3m1 (156)	0.165	0.132	C	Γ→M	0.13	1.627	False
BiBrTe	304bc6a92d82	P3m1 (156)	0.0	0.878	V	Γ→K	0.001	0.065	False
ZrO2	24a8929c68ce	P-6m2 (187)	0.766	1.683	C	M→K	0.065	0.026	False
AsIS	e23390b66883	P3m1 (156)	0.256	0.295	C	M→K	0.016	0.65	False
Hf2Zr2Te8	93099006c996	P1 (1)	0.121	0.189	V	Y→S	0.012	0.375	False
					V	Γ→S	0.02	0.189	False
W2I6	37deba64dc68	P-62m (189)	0.19	0.205	V	Γ→M	0.018	0.0	False
					V	M→Γ	0.018	0.0	False
					C	M→Γ	0.085	0.258	False
GeF2	943ceb2df00b	P-4m2 (115)	0.215	1.623	V	Γ→X	0.001	1.956	False
WMo3Te8	323fb700d903	P1 (1)	0.005	0.923	V	Y→S	0.008	0.423	False
					V	S→Γ	0.21	0.192	False
					C	Γ→X	0.014	0.0	False
					C	X→Γ	0.014	0.0	False
					C	Γ→S	0.03	0.222	False
AsIS	b13beafa16aa	P3m1 (156)	0.064	1.395	V	Γ→K	0.135	0.079	True
WCr3Se8	c798e725e2fb	P1 (1)	0.009	0.698	V	Y→S	0.046	0.499	False
					V	S→Γ	0.117	0.173	False
AsBiCr	b299416bff28	P3m1 (156)	0.461	0.037	C	M→Γ	0.039	0.0	False
BaBr2	df54a81e64da	P-4m2 (115)	0.244	4.568	C	X→M	0.03	0.719	False
Ga2Se2	394e5709a3ac	P-6m2 (187)	0.0	1.736	C	M→K	0.063	1.04	False
MoW3Se8	24d6cc0a0fed	Pm (6)	0.0	1.276	V	S→Γ	0.245	0.293	False
					C	X→Γ	0.018	0.0	False
GaN	c973e283b023	P-6m2 (187)	0.416	1.818	V	Γ→K	0.019	1.549	False

Formula	Entry Info C2DB ID	SG index	ΔE_{hull}	Bandgap	Spin Splitting Info Band	k-point	ΔE_{SS}	$\Delta E_{VBM/CBM}$	AC
Cr2Mo2S8	72b286460831	Pma2 (28)	0.017	1.039	C	S→Γ	0.024	0.305	False
HfZr3Te8	916e19eae465	P1 (1)	0.115	0.242	V	S→X	0.005	0.367	False
					V	S→Y	0.029	0.228	False
					V	Y→S	0.009	0.33	False
					V	Γ→S	0.019	0.242	False
					C	X→Γ	0.037	0.02	False
					C	S→X	0.002	0.2	False
ISSb	4c49d27e66e5	P3m1 (156)	0.185	0.872	C	M→K	0.057	0.469	False
GeI2	694ac91aec01	P-4m2 (115)	0.153	1.059	V	Γ→M	0.309	0.0	False
					V	Γ→X	0.139	0.532	False
					C	Γ→M	0.008	1.342	False
					C	Γ→X	0.036	1.45	False
					C	M→X	0.003	1.309	False
Rh2Br6	c284d6de2b3e	P3 (143)	0.408	0.26	V	K→Γ	0.003	0.001	False
ClSSb	9188c300265c	P3m1 (156)	0.048	1.332	V	Γ→M	0.006	0.045	False
					V	M→Γ	0.006	0.045	False
					V	Γ→K	0.01	0.0	False
					C	M→K	0.312	1.879	False
HfO2	6e4ac7453419	P-4m2 (115)	0.51	4.494	V	X→Γ	0.008	0.628	False
					C	Γ→M	0.184	1.209	False
					C	Γ→X	0.156	0.782	False
SnTe	e688959ea45b	P3m1 (156)	0.119	1.592	C	M→Γ	0.025	0.0	False
HfCl2	864f8b497185	P-6m2 (187)	0.007	0.891	C	M→K	0.15	1.596	False
GeCl2	3ea474649fa9	P-4m2 (115)	0.143	1.381	V	Γ→M	0.002	0.0	False
					V	Γ→X	0.027	1.107	False
					V	X→M	0.002	0.0	False
					C	Γ→M	0.056	1.708	False
ZnBr2	4718298eb660	P-4m2 (115)	0.0	3.278	V	X→M	0.012	4.046	False
					C	Γ→M	0.099	1.754	False
					C	Γ→X	0.017	0.768	False
					C	X→M	0.065	1.685	False
ClIZr	73202b4b7837	P3m1 (156)	0.078	0.883	C	M→K	0.013	0.92	False
P2Sc2Se6	093920d00119	P3 (143)	0.0	0.68	V	Γ→M	0.032	0.0	False
					V	M→Γ	0.032	0.0	False
					V	K→M	0.032	0.0	False
					V	K→Γ	0.031	0.005	False
					V	Γ→K	0.031	0.005	False
					C	Γ→M	0.013	0.29	False
					C	K→Γ	0.008	0.279	False
					C	Γ→K	0.008	0.279	False
Ti2Zr2Se8	846b50801a93	P1 (1)	0.142	0.616	C	X→Γ	0.025	0.149	False
TiHf3S8	eb71cb1c9077	P1 (1)	0.205	1.005	V	X→S	0.017	0.15	False
					V	Y→S	0.025	0.016	False
					V	Y→Γ	0.008	0.111	False
					C	X→Γ	0.028	0.033	False
					C	X→S	0.002	0.091	False
					C	Γ→Y	0.009	0.0	False
GeTe	eadd37f03ca5	P3m1 (156)	0.087	1.488	C	M→Γ	0.043	0.0	False
					C	M→K	0.233	0.813	True
Ir2Cl6	be7870547213	P321 (150)	0.555	0.263	V	M→Γ	0.002	0.0	False
					C	M→Γ	0.001	0.071	False
S2Si2	0726c763a59a	$Pmn2_1$(31)	0.446	1.433	C	S→Y	0.006	0.082	False
					C	Y→Γ	0.012	0.0	False
					C	S→Γ	0.005	0.879	False
BaCl2	ef1fab58e11f	P-4m2 (115)	0.3	5.195	C	X→M	0.031	0.724	False
OSn	026ebfd86b48	P3m1 (156)	0.329	1.682	C	Γ→M	0.102	1.698	False

Formula	Entry Info C2DB ID	SG index	ΔE_{hull}	Bandgap	Spin Splitting Info Band	k-point	ΔE_{SS}	$\Delta E_{VBM/CBM}$	AC
					C	M→Γ	0.102	1.698	False
					C	Γ→K	0.071	2.315	False
SnTe2	c81de95356c1	P-4m2 (115)	0.139	0.39	V	X→Γ	0.088	0.171	False
					V	X→M	0.015	0.171	False
					C	Γ→M	0.344	0.876	False
					C	Γ→X	0.096	0.22	False
AsClS	0fd6ab210774	P3m1 (156)	0.224	1.732	C	M→K	0.05	0.414	False
W2Br6	14e114b103e1	P-62m (189)	0.271	0.222	C	M→Γ	0.077	0.375	False
Ir2S2	dd6289af8e01	P-6m2 (187)	0.305	0.135	C	Γ→K	0.029	1.386	False
CaI2	793f311ee701	P-4m2 (115)	0.174	4.022	C	Γ→M	0.012	0.388	False
MoCr3Te8	899032b4ad0c	P1 (1)	0.087	0.481	V	S→Γ	0.097	0.137	False
BiIS	40034665f9f1	P3m1 (156)	0.14	0.848	C	M→K	0.333	0.539	False
GaP	d467820f3f04	P3m1 (156)	0.447	1.555	C	M→Γ	0.01	1.217	False
					C	M→K	0.01	0.625	False
Al2S2	f9df9f4a5c34	P-6m2 (187)	0.005	2.099	V	M→K	0.012	0.649	False
HfSSe	63618e5bf062	P3m1 (156)	0.0	0.705	C	Γ→M	0.019	0.794	False
					C	Γ→K	0.065	0.959	False
ZrBr2	7897c7cc2491	P-6m2 (187)	0.0	0.827	C	M→K	0.01	1.413	False
AsBrSe	989f469f06bd	P3m1 (156)	0.0	1.212	C	M→Γ	0.005	0.982	False
HgSe	619ed885f677	P3m1 (156)	0.157	0.069	V	Γ→M	0.01	0.007	False
					V	M→Γ	0.048	0.899	False
					V	Γ→K	0.023	0.0	False
BiITe	a84d988e38ac	P3m1 (156)	0.11	0.691	V	Γ→K	0.029	0.165	False
AsBrTe	64921449e408	P3m1 (156)	0.0	1.253	V	Γ→M	0.092	0.023	False
					V	Γ→K	0.105	0.0	False
					C	Γ→M	0.02	0.838	False
SSeZr	1a9901838600	P3m1 (156)	0.0	0.616	C	Γ→M	0.005	0.609	False
					C	Γ→K	0.024	0.831	False
GeCl2	a7216f084785	P-6m2 (187)	0.136	2.955	C	M→K	0.045	0.089	False
O2Pb2	20f098bd3f31	Pm (6)	0.287	0.215	V	Y→S	0.03	0.155	False
					V	Y→Γ	0.091	0.138	False
SSeZr	2be14f373da0	P3m1 (156)	0.163	0.831	V	Γ→K	0.105	0.0	False
					C	Γ→M	0.003	0.0	False
					C	Γ→K	0.063	0.086	False
BrSbSe	89b15ddef41d	P3m1 (156)	0.0	1.072	V	M→Γ	0.036	0.035	False
					V	M→K	0.044	0.383	False
PbSe	a0dbdc6630fa	P3m1 (156)	0.217	1.68	V	Γ→M	0.047	0.002	False
					V	M→Γ	0.047	0.002	False
					V	Γ→K	0.053	0.0	False
					C	Γ→M	0.293	0.542	False
					C	Γ→K	0.346	0.887	False
GeS2	69b36b84eb8c	P-4m2 (115)	0.049	1.36	V	Γ→X	0.003	0.382	False
					C	Γ→M	0.038	1.504	False
					C	X→M	0.028	0.97	False
HfSeTe	305c779b8752	P3m1 (156)	0.149	0.16	C	Γ→M	0.014	0.0	False
					C	Γ→K	0.212	0.298	False
SnCl2	95805103ce95	P-4m2 (115)	0.146	1.464	V	Γ→M	0.002	0.0	False
					V	Γ→X	0.02	1.116	False
					V	X→M	0.002	0.0	False
Pb2Te2	fdc4a7cc1d0d	$Pmn2_1$(31)	0.075	0.701	V	S→Y	0.003	0.213	False
					V	Y→S	0.003	0.213	False
HfTi3Se8	c55716558616	P1 (1)	0.137	0.589	V	S→X	0.012	0.268	False
					C	X→Γ	0.015	0.025	False
					C	Y→Γ	0.002	0.064	False
AlSb	1734deee2ac1	P3m1 (156)	0.475	1.447	V	Γ→M	0.018	0.969	False
					V	M→Γ	0.018	0.969	False

Formula	Entry Info C2DB ID	SG index	ΔE_{hull}	Bandgap	Spin Splitting Info Band	k-point	ΔE_{SS}	$\Delta E_{VBM/CBM}$	AC
					V	Γ→K	0.011	1.117	False
					C	Γ→M	0.129	0.855	False
					C	Γ→K	0.223	1.151	False
Mo2W2Te8	c04fc052f2ca	Pm (6)	0.011	0.879	V	Y→S	0.022	0.477	False
					V	S→Γ	0.217	0.224	False
					C	X→Γ	0.01	0.0	False
BiISe	70cbc0e44d36	P3m1 (156)	0.0	0.929	V	Γ→K	0.037	0.206	True
GeO	a42f736f1682	P3m1 (156)	0.311	2.093	V	Γ→M	0.006	0.437	False
					C	Γ→M	0.002	2.191	False
					C	M→Γ	0.002	2.191	False
					C	M→K	0.057	0.759	False
					C	Γ→K	0.071	2.677	False
Pb2Te6	3995fa1bee6e	$P2_1(4)$	0.129	0.322	V	S→X	0.009	0.0	False
					V	S→Γ	0.063	0.024	False
					C	Y→Γ	0.026	0.759	False
					C	Γ→Y	0.04	0.781	False
Mo2Cl6	61d74efeaeeb	P-62m (189)	0.139	0.526	C	M→Γ	0.03	0.372	False
BrSSb	4ae37f15e1fe	P3m1 (156)	0.157	1.437	C	M→Γ	0.042	0.533	False
					C	M→K	0.1	0.357	False
ZrTe2	599f0c912458	P-4m2 (115)	0.373	0.816	V	Γ→M	0.112	0.858	False
					V	Γ→X	0.065	0.882	False
					V	X→M	0.065	0.882	False
					C	M→Γ	0.034	0.0	False
					C	X→M	0.038	0.044	False
Cr2W2S8	5974b6403c31	Pma2 (28)	0.014	0.967	C	X→Γ	0.009	0.0	True
					C	Y→S	0.025	0.199	False
HfZr3Se8	70e7ab872359	P1 (1)	0.15	0.819	V	X→S	0.01	0.214	False
					V	Y→Γ	0.003	0.09	False
					V	Γ→Y	0.003	0.09	False
					C	X→Γ	0.018	0.039	False
					C	X→S	0.004	0.137	False
					C	S→Y	0.03	0.041	False
HfSe2	08401460f377	P-4m2 (115)	0.337	1.676	V	Γ→M	0.081	0.718	False
					V	Γ→X	0.064	0.74	False
					V	X→M	0.064	0.74	False
					C	M→Γ	0.116	0.0	False
					C	M→X	0.148	0.012	False
Rh2Se2	1a46a7cf8fab	P-6m2 (187)	0.164	0.063	V	M→K	0.105	0.653	False
AsClSe	df329350eef2	P3m1 (156)	0.179	1.71	C	M→K	0.075	0.402	False
GeSe	211bcb7f05d6	P3m1 (156)	0.04	2.215	V	Γ→M	0.003	0.111	False
					V	M→Γ	0.072	0.054	False
					C	Γ→M	0.094	0.767	False
					C	M→K	0.104	0.611	False
					C	Γ→K	0.162	0.908	False
TiZr3S8	ec37c6657ea3	P1 (1)	0.184	0.997	V	Y→S	0.016	0.039	False
					V	Y→Γ	0.005	0.107	False
					C	X→Γ	0.006	0.052	False
					C	Y→Γ	0.003	0.0	False
Al2P2Se6	90d84f697622	P1 (1)	0.067	0.607	V	Γ→Y	0.056	0.0	False
					V	Γ→X	0.056	0.001	False
					C	Γ→Y	0.064	0.588	False
					C	Γ→X	0.063	0.589	False
Hf2Zr2Se8	81af2831dbb2	P1 (1)	0.158	0.845	C	X→Γ	0.036	0.025	False
MoW3Te8	5c3fe56a1a89	Pm (6)	0.018	0.825	V	Y→S	0.014	0.546	False
					V	S→Γ	0.239	0.254	False
Mo2W2S8	449640ec4d30	Pc (7)	0.0	1.553	C	X→Γ	0.013	0.0	True

Entry Info					Spin Splitting Info				
Formula	C2DB ID	SG index	ΔE_{hull}	Bandgap	Band	k-point	ΔE_{SS}	$\Delta E_{VBM/CBM}$	AC
HfTi3S8	fde2d81d10df	P1 (1)	0.169	0.848	V	S→X	0.009	0.154	False
					V	Y→S	0.02	0.014	False
					C	X→Γ	0.009	0.036	False
HgCl2	ce3ed4728e8f	P-4m2 (115)	0.033	2.404	C	X→M	0.001	0.0	False
GeBr2	204ef2affa10	P-4m2 (115)	0.136	1.312	C	Γ→M	0.007	1.599	False
Ga2Cl6	c306553fa81a	P-62m (189)	0.174	2.553	V	Γ→M	0.02	0.0	False
BrClHf	72257f9ad66d	P3m1 (156)	0.016	0.819	V	Γ→M	0.01	0.802	False
					V	Γ→K	0.018	0.793	False
					C	M→K	0.119	1.4	False
AsClS	afd0d75a82a2	P3m1 (156)	0.056	1.532	V	Γ→M	0.005	0.044	False
					V	M→K	0.018	0.465	False
					V	Γ→K	0.005	0.0	False
					C	Γ→M	0.016	0.935	False
					C	M→K	0.096	1.787	False
TiO2	1cfb690281c9	P-6m2 (187)	0.587	1.136	C	M→K	0.031	0.121	False
P2Sc2S6	bc8b8c21ad4f	P3 (143)	0.08	0.829	V	Γ→Y	0.007	0.0	False
					V	Γ→X	0.007	0.0	False
CrMo3S8	644f7c1c85c7	Pm (6)	0.011	1.206	V	S→Y	0.075	0.557	False
					C	Γ→X	0.011	0.0	False
					C	Γ→S	0.001	0.216	False
					C	S→Γ	0.011	0.278	False
OPb	2a393480e273	P3m1 (156)	0.315	1.806	V	Γ→M	0.017	0.032	False
					V	Γ→K	0.019	0.0	False
InSb	466fcf7fad66	P3m1 (156)	0.379	0.477	V	Γ→M	0.031	0.991	False
					V	M→Γ	0.031	0.991	False
					V	Γ→K	0.091	1.082	False
					C	Γ→M	0.187	1.174	False
					C	Γ→K	0.283	1.414	False
AsClTe	4fd8ad708fb0	P3m1 (156)	0.018	1.496	C	M→K	0.097	1.188	False
					C	Γ→K	0.038	1.159	False
CrW3Te8	eef072f845ce	P1 (1)	0.056	0.563	V	S→Γ	0.204	0.223	False
MoCr3S8	3fb52099b370	P1 (1)	0.011	0.922	C	X→Γ	0.006	0.0	False
					C	S→Γ	0.007	0.398	False
BiBrS	3b305c3e2c18	P3m1 (156)	0.116	1.594	C	M→K	0.321	0.478	False
CrW3Se8	0b7696e1f4c9	P1 (1)	0.01	0.902	V	S→Γ	0.191	0.256	False
PdSe2	0ae696751911	P-6m2 (187)	0.268	0.231	V	Γ→K	0.344	1.632	False
TiHf3Te8	1667d1443160	P1 (1)	0.132	0.098	V	Γ→X	0.003	0.513	False
					V	S→X	0.004	0.475	False
					V	Γ→S	0.017	0.098	False
Ti2Zr2Te8	18e377cce57f	P1 (1)	0.118	0.143	V	Γ→S	0.022	0.143	False
					C	X→Γ	0.05	0.25	False
N2O2Zr3	c317fbd68215	P-6m2 (187)	0.094	0.404	C	Γ→K	0.019	0.385	False
PbS	5e4ff1f56b4a	P3m1 (156)	0.231	1.979	C	Γ→M	0.295	0.542	False
					C	M→K	0.268	0.681	False
					C	Γ→K	0.347	0.801	False
Ge2S2	ecbb7c185669	$Pmn2_1$(31)	0.031	1.714	C	Y→Γ	0.056	0.0	False
InP	c5672c6c1c78	P3m1 (156)	0.432	1.072	V	Γ→M	0.017	1.008	False
					V	M→Γ	0.017	1.008	False
					V	Γ→K	0.01	1.098	False
					C	Γ→M	0.01	1.378	False
					C	M→Γ	0.01	1.378	False
					C	M→K	0.017	1.1	False
					C	Γ→K	0.029	1.724	False
SeTeZr	dd69b684c867	P3m1 (156)	0.115	0.275	C	Γ→M	0.009	0.0	False
					C	M→Γ	0.009	0.0	False
					C	Γ→K	0.094	0.198	False

Entry Info					Spin Splitting Info				
Formula	C2DB ID	SG index	ΔE_{hull}	Bandgap	Band	k-point	ΔE_{SS}	$\Delta E_{VBM/CBM}$	AC
Hf2Ti2S8	c8cfffe63bfa	P1 (1)	0.192	0.917	V	X→S	0.006	0.19	False
					V	Y→S	0.027	0.0	False
					C	X→Γ	0.013	0.026	False
					C	X→S	0.001	0.09	False
PbTe	3bc08d486d65	P3m1 (156)	0.198	1.151	C	Γ→M	0.349	0.383	False
					C	Γ→K	0.398	0.869	False
ZrTi3S8	e6e376c80c43	P1 (1)	0.163	0.833	V	S→X	0.01	0.147	False
					V	Y→S	0.016	0.029	False
					C	X→Γ	0.002	0.036	False
CdI2	d63ad801fdb5	P-4m2 (115)	0.0	2.381	V	X→M	0.018	0.0	False
AsBrS	d9f4d4011670	P3m1 (156)	0.201	1.425	C	M→Γ	0.04	0.481	False
					C	M→K	0.018	0.52	False
TiZr3Te8	4f1ab08988cc	P1 (1)	0.115	0.21	C	X→Γ	0.026	0.247	False
MoSTe	e4bb8738150a	P3m1 (156)	0.065	1.027	V	M→Γ	0.006	0.917	False
TiHf3Se8	3e1923c616ad	P1 (1)	0.166	0.722	V	Γ→X	0.021	0.037	False
					V	X→S	0.018	0.228	False
					C	Y→Γ	0.006	0.062	False
CrO2	2433700165bb	P-6m2 (187)	0.168	0.422	V	M→K	0.049	1.259	False
Cr2Mo2Se8	60065d3bbcf2	P1 (1)	0.016	0.837	V	S→Γ	0.1	0.158	False
					C	X→Γ	0.012	0.0	False
					C	S→Γ	0.002	0.29	False
CrMo3Se8	a7233837cfe9	P1 (1)	0.01	0.971	V	S→Γ	0.115	0.185	False
					C	Γ→X	0.018	0.0	False
					C	S→Γ	0.004	0.253	False
Ti2Zr2S8	a99139546333	P1 (1)	0.18	0.842	V	S→X	0.005	0.205	False
					V	S→Y	0.021	0.0	False
					V	Y→S	0.021	0.0	False
ZrHf3Se8	b8fb10416122	P1 (1)	0.165	0.843	V	Y→Γ	0.002	0.083	False
					C	X→Γ	0.044	0.021	False
					C	X→S	0.002	0.167	False
					C	S→Y	0.036	0.004	False
ClSSb	0495f35048b5	P3m1 (156)	0.179	1.675	V	Γ→M	0.01	0.099	False
					V	M→Γ	0.01	0.099	False
					V	Γ→K	0.034	0.0	False
					C	M→K	0.135	0.292	False
Hf2Ti2Se8	cce78d90e899	P1 (1)	0.156	0.656	V	Γ→X	0.021	0.029	False
					V	X→S	0.002	0.236	False
					V	Γ→S	0.03	0.024	False
					C	X→Γ	0.021	0.053	False
					C	X→S	0.022	0.0	False
SnS2	08a9307b286e	P-4m2 (115)	0.082	1.451	V	Γ→X	0.004	0.258	False
					C	M→Γ	0.034	1.351	False
					C	Γ→M	0.034	1.351	False
					C	Γ→X	0.007	0.427	False
					C	X→Γ	0.007	0.427	False
					C	M→X	0.027	1.123	False
SnSe2	bfa429d647f9	P-4m2 (115)	0.056	0.854	V	X→M	0.006	1.212	False
					C	Γ→M	0.157	1.191	False
					C	Γ→X	0.024	0.358	False
PbS2	9842835dff03	P-4m2 (115)	0.418	0.671	V	M→Γ	0.002	0.169	False
					V	M→X	0.002	0.0	False
					C	X→M	0.033	0.896	False
WMo3Se8	05a06afa3b20	Pm (6)	0.0	1.32	V	S→Γ	0.195	0.232	False
					C	Γ→X	0.01	0.0	False
					C	X→Γ	0.01	0.0	False
					C	Y→S	0.025	0.124	False

Entry Info					Spin Splitting Info				
Formula	C2DB ID	SG index	ΔE_{hull}	Bandgap	Band	k-point	ΔE_{SS}	$\Delta E_{VBM/CBM}$	AC
O2W2	42fa50003592	P-6m2 (187)	0.503	0.04	V	Γ→K	0.163	0.0	False
BrSSb	4da5c6be60db	P3m1 (156)	0.028	1.233	V	M→Γ	0.061	0.056	False
Cr2W2Se8	548aa830244c	P1 (1)	0.015	0.778	V	S→Γ	0.153	0.195	False
					C	Y→S	0.009	0.187	False
ZnCl2	1b7175e04416	P-4m2 (115)	0.0	4.226	V	Γ→X	0.003	0.936	False
					C	Γ→M	0.016	2.096	False
					C	Γ→X	0.011	2.084	False
					C	X→M	0.011	2.084	False
TiZr3Se8	a148361e5e9a	P1 (1)	0.144	0.701	V	Y→Γ	0.002	0.112	False
					C	X→Γ	0.012	0.043	False
Al2Se2	129a514b51ad	P-6m2 (187)	0.0	1.997	C	M→K	0.034	0.328	False
GeS	227b12019ade	P3m1 (156)	0.053	2.467	C	Γ→M	0.057	1.039	False
					C	M→K	0.036	0.509	False
					C	Γ→K	0.078	1.141	False
BiClS	c96ef4fc869c	P3m1 (156)	0.0	1.334	V	Γ→M	0.01	0.031	True
					V	Γ→K	0.018	0.0	False
Ga2P2Te6	4cb4ea247ef4	P1 (1)	0.173	0.314	V	Γ→Y	0.022	0.406	False
					V	Γ→X	0.017	0.405	False
AsITe	b6d803aafe3a	P3m1 (156)	0.0	1.009	V	Γ→M	0.001	0.335	False
					V	M→K	0.059	0.779	False
					V	Γ→K	0.051	0.311	False
AsClSe	1a3be826b3e0	P3m1 (156)	0.013	1.364	C	M→K	0.073	1.703	False
HfTe2	1e2c6946ca41	P-4m2 (115)	0.371	1.01	V	Γ→M	0.147	0.78	False
					V	Γ→X	0.119	0.798	False
					V	X→M	0.119	0.798	False

References

[1] Sten Haastrup et al. "The Computational 2D Materials Database: high-throughput modeling and discovery of atomically thin crystals". In: *2D Materials* 5 (4 Sept. 2018), p. 042002. ISSN: 2053-1583. DOI: 10.1088/2053-1583/AACFC1.